JOURNAL OF PETROLOGY | VOLUME 55 | NUMBER 1 | PAGES 37–62 | 2014 | doi:10.1093/petrology/egt060

Geological and Geochemical Evolution of the Quaternary Süphan Stratovolcano, Eastern Anatolia, Turkey: Evidence for the Lithosphere–Asthenosphere Interaction in Post-Collisional Volcanism

YAVUZ ÖZDEMİR[1,2]* AND NİLGÜN GÜLEÇ[2]

[1]DEPARTMENT OF GEOLOGICAL ENGINEERING, YUZUNCU YIL UNIVERSITY, 65080, VAN, TURKEY

[2]DEPARTMENT OF GEOLOGICAL ENGINEERING, MIDDLE EAST TECHNICAL UNIVERSITY, 06531 ANKARA, TURKEY

RECEIVED JUNE 24, 2012; ACCEPTED SEPTEMBER 23, 2013
ADVANCE ACCESS PUBLICATION NOVEMBER 13, 2013

The Süphan stratovolcano is one of the major Quaternary eruption centers of post-collisional volcanism in eastern Anatolia, located in the zone of convergence between the Arabian and the Anatolian plates. We document the geological and geochemical evolution of Süphan in terms of volcanostratigraphy, geochronology (^{40}Ar–^{39}Ar), isotope composition (Sr, Nd, Pb) and bulk-rock geochemistry. Our new ^{40}Ar–^{39}Ar data, along with previously published K/Ar ages, indicate an age of 0·76–0·06 Ma for the eruptive products, which extend over an area of ~2000 km^2. The products of Süphan include transitional mildly alkaline to calc-alkaline lavas, domes and pyroclastic rocks ranging in composition from basalt to rhyolite. MELTS modeling suggests that the majority of the Süphan magmas with SiO_2 contents between ~57 and ~65 wt % are the products of isobaric–isenthalpic mixing of basaltic trachyandesitic and rhyolitic magmas at a crustal pressure of 0·5 kbar. Energy-constrained assimilation and fractional crystallization modeling of trace element and isotope compositions points to 2–10% (upper) crustal contamination that accompanied differentiation. Large ion lithophile element enrichment and the presence of negative high field strength element anomalies in primitive mantle-normalized trace element patterns suggest a mantle source that was modified by subducted sediments. Light to heavy and medium to heavy rare earth element ratios and partial melting models suggest the derivation of the eastern Anatolian parental magmas from variable mixing of lithospheric and asthenospheric melts. Unlike the commonly accepted models for post-collisional volcanism that envisage an increasing contribution from asthenospheric melts with time, melting degree and contribution of the lithospheric mantle seem to have increased from Miocene–Pliocene to Quaternary times in eastern Anatolia.

KEY WORDS: *eastern Anatolia; Süphan volcano; post-collisional magmatism*

INTRODUCTION

The Eastern Anatolian Plateau (EAP) has formed as part of a Turkic-type orogenic system through the convergence of the Arabian and Anatolian (Eurasian) plates (Şengör *et al.*, 2008). This collision caused intense seismic activity, strike-slip fault zones (right-lateral North Anatolian Fault Zone and left-lateral East Anatolian Fault Zone), westward movement of the Anatolian plate and widespread Late Cenozoic volcanism. The nature of the tectonism in the region reveals a transition from a north–south-directed compressional–contractional regime (post-collisional convergence) in Middle Miocene–Early Pliocene times to a compressional–extensional regime (tectonic escape) in Early Pliocene–Recent times (Koçyiğit *et al.*, 2001). Shallow and diffuse seismicity (e.g. the recent M = 7·2

*Corresponding author. Present address: Department of Geological Engineering, Yuzuncu Yıl University, 65080, Van, Turkey. Telephone: (+) 90 432 2251732. Fax: (+) 90 432 2251732.
E-mail: yozdemir@yyu.edu.tr, yavuzozde@gmail.com

© The Author 2013. Published by Oxford University Press. All rights reserved. For Permissions, please e-mail: journals.permissions@oup.com

Downloaded from https://academic.oup.com/petrology/article-abstract/55/1/37/1524170 by Yuzuncu Yil University user on 23 April 2020

Van earthquake of 23 October 2011) in the region indicates that the eastern Anatolian lithosphere is still being actively deformed as a result of continuing collision and crustal escape tectonics.

The age of the initial contact between Arabia and Eurasia has not yet been determined conclusively. Reported ages for the collision range from Late Cretaceous (Hall, 1976; Berberian & King, 1981; Alavi, 1994), through Late Eocene–Oligocene (35–25 Ma; Jolivet & Faccenna, 2000; Agard *et al.*, 2005; Allen & Armstrong, 2008), to Miocene (Şengör *et al.*, 1985, 2008; Dewey *et al.*, 1986; Yılmaz, 1993; Robertson *et al.*, 2007). Recently Okay *et al.* (2010) pointed out that the last oceanic lithosphere between the Arabian and Eurasian plates was consumed by the Early Miocene (~20 Ma) based on apatite fission-track ages of metamorphic rocks and Eocene sandstones from the Bitlis–Zagros Thrust Zone. Subsequent to the onset of collision the continuing convergence along the Bitlis Sture Zone (Fig. 1a) has given rise to uplift of the EAP (Şengör & Kidd, 1979). At present, the EAP has an average elevation of ~2 km, and is composed of several microcontinents accreted to each other, separated by ophiolite belts and accretionary complexes (Şengör, 1990). The basement rocks of these microcontinents are unconformably overlain by Oligocene to Miocene shallow marine deposits and Late Cenozoic collision-related volcanic rocks. Products of the post-collision volcanism span the Arabian foreland in the south to the Erzurum–Kars Plateau in the north (e.g. Yılmaz *et al.*, 1987, 1998; Pearce *et al.*, 1990; Notsu *et al.*, 1995; Keskin *et al.*, 1998; Keskin, 2003, 2007; Karaoğlu *et al.*, 2005; Özdemir *et al.*, 2006, 2007, 2011; Oyan, 2011), with a series of large shield volcanoes (e.g. Tendürek) and stratovolcanoes (e.g. Ağrı, Nemrut, Süphan, Etrüsk, Fig. 1a).

The origin and time–space distribution of the collision-related volcanism still remain matters of debate, and many models have been put forward. These petrogenetic models can be divided into two main groups: in the first group, the magmas are considered to have originated by partial melting of the lithospheric mantle (e.g. Pearce *et al.*, 1990; Yılmaz *et al.*, 1998; Şen *et al.*, 2004); in the second group, the source region of the magmas is regarded as the asthenosphere, with or without a subduction component related to the steepening and break-off of a northward subducting slab belonging to the northern branch of the Neo-Tethyan ocean (e.g. Keskin, 2003, 2007; Şengör *et al.*, 2003, 2008).

Testing the validity of these geodynamic models requires detailed volcanological, geochemical and geochronological investigation of the eruptive products from each volcanic center in the region. Our study focuses on Süphan, one of the least known Quaternary volcanoes in eastern Anatolia. We document the volcanostratigraphy of Süphan based on detailed investigations of pyroclastic deposits and lavas combined with new ^{40}Ar–^{39}Ar ages. A combination of our previously published whole-rock (Özdemir *et al.*, 2011) and new Sr–Nd–Pb isotope data is used to interpret the chemical variations of the Süphan magmas in terms of fractional crystallization, magma mixing, crustal contamination and mantle sources. Additionally, we use previously published geochemical data for the most mafic volcanic rocks from eastern Anatolia to propose a new model for the source(s) of the parental magmas.

METHODS

A geological map of an area of ~1100 km^2 was prepared based on 1:25 000 scale topographic maps. Aerial photographs (at a scale of 1:35 000) and digital elevation models (DEM, at a scale of 1:25 000) were utilized in the field to help distinguish the boundaries of lava flows, and to identify secondary eruption centers and structural features. Electron microprobe analysis (EMPA) was undertaken at the University of Bristol using a CAMECA SX-100 five-spectrometer (wavelength-dispersive spectrometry; WDS) instrument. Whole-rock major element compositions (Supplementary Material 1; all supplementary material is available for downloading at http://www.petrology.oxfordjournals.org) were determined by inductively coupled plasma emission spectrometry (ICP-ES) following lithium metaborate/tetraborate fusion and dilute nitric acid digestion at ACME (Canada) analytical laboratories. Trace element contents (Supplementary Material 1) were determined in the same laboratory by inductively coupled plasma mass spectrometry (ICP-MS) following lithium metaborate/tetraborate fusion and nitric acid digestion.

Sr (22 samples), Nd (21 samples) and Pb (20 samples) isotopic analyses of selected Süphan volcanic rocks were carried out at the Pacific Centre for Isotopic and Geochemical Research (PCIGR) at the University of British Columbia (UBC). Sr and Nd isotope ratios were measured by thermal ionization mass spectrometry (TIMS) on a Thermo Finnigan Triton system. Sr and Nd isotopic compositions were corrected for mass fractionation using $^{86}Sr/^{88}Sr = 0{\cdot}1194$ and $^{146}Nd/^{144}Nd = 0{\cdot}7219$. During the period when the Süphan samples were analyzed, the international Nd standard La Jolla gave an average value of $0{\cdot}511856 \pm 0{\cdot}000021$ (2σ; $n = 4$) and international Sr standard SRM 987 gave an average of $0{\cdot}710244 \pm 0{\cdot}000020$ (2σ; $n = 5$). US Geological Survey (USGS) reference material USGS-G2 was processed with the samples and yielded Sr and Nd isotopic ratios of 0·709755 and 0·512222, respectively. These are in agreement with the published values of $0{\cdot}709770 \pm 14$ and $0{\cdot}512228 \pm 6$, respectively (Weis *et al.*, 2006).

Pb isotopic compositions were analyzed by multiple collector–inductively coupled plasma–mass spectrometry (MC-ICP-MS) on a Nu Plasma (Nu Instruments) system. The detailed analytical procedure for Pb isotopic analyses

Downloaded from https://academic.oup.com/petrology/article-abstract/55/1/37/1524170 by Yuzuncu Yil University user on 23 April 2020

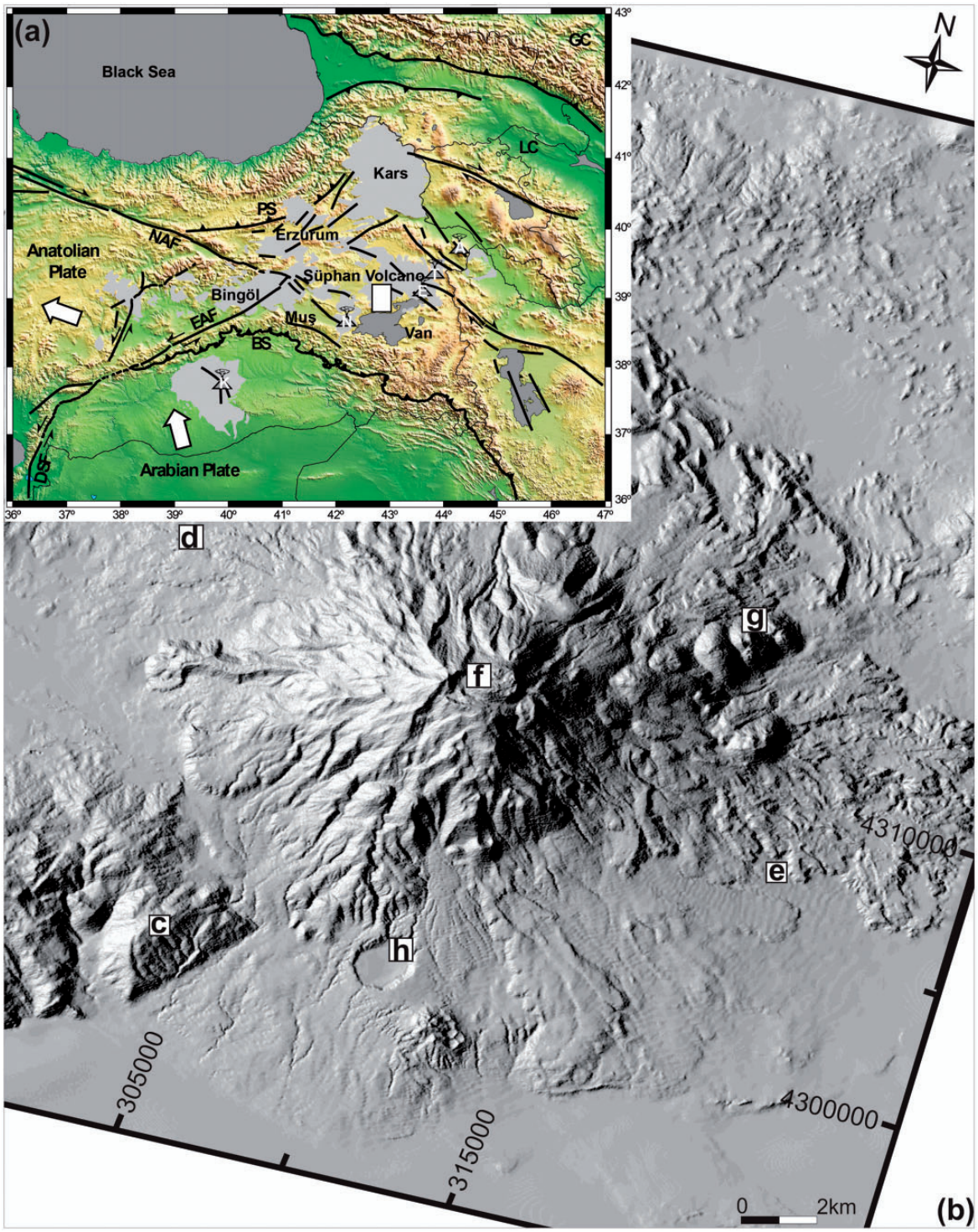


Fig. 1. (a) Map showing the tectonic setting of eastern Anatolia, topographic relief and locations of collision-related volcanic rocks (light grey). NAF, North Anatolian Fault; EAF, East Anatolian Fault; DSF, Dead Sea Fault; BS, Bitlis Suture; PS, Pontide Suture; LC, Lesser Caucasus; GC, Greater Caucasus; K, Karacadağ Volcano; N, Nemrut Volcano; E, Etrüsk Vocano; T, Tendürek Volcano; A, Ağrı Volcano (modified from Özacar *et al.*, 2008). (b) Shaded relief map of the Süphan stratovolcano, showing the morphology and distribution of volcanic products. (c) Miocene shallow marine, dolomitized limestones (Adilcevaz Limestone) over which the products of the Süphan volcanism were emplaced in the western and southwestern parts of the volcano. (d) Late basaltic trachyandesitic (LBTA) and early trachyandesitic (ETA) flows, which are the most widespread lava flows and extend over an area of ~150 km^2 in the western, northern and northeastern parts of the volcano. (e) Block and ash flow with radially fractured blocks, forming one of the most common pyroclastic deposits around Süphan; the size of the blocks is up to 1·5 m in the vicinity of the main cone. (f, g) Dacitic and rhyolitic domes that were extruded after the lavas and pyroclastic deposits of the main cone and are situated on the summit (f) and on the flanks (g) of the volcano. (h) Aygır maar in the southern part of the volcano, constituting the most recent product of Süphan volcanism with a circular crater of diameter 1·5 km.

(continued)

Downloaded from https://academic.oup.com/petrology/article-abstract/55/1/37/1524170 by Yuzuncu Yil University user on 23 April 2020

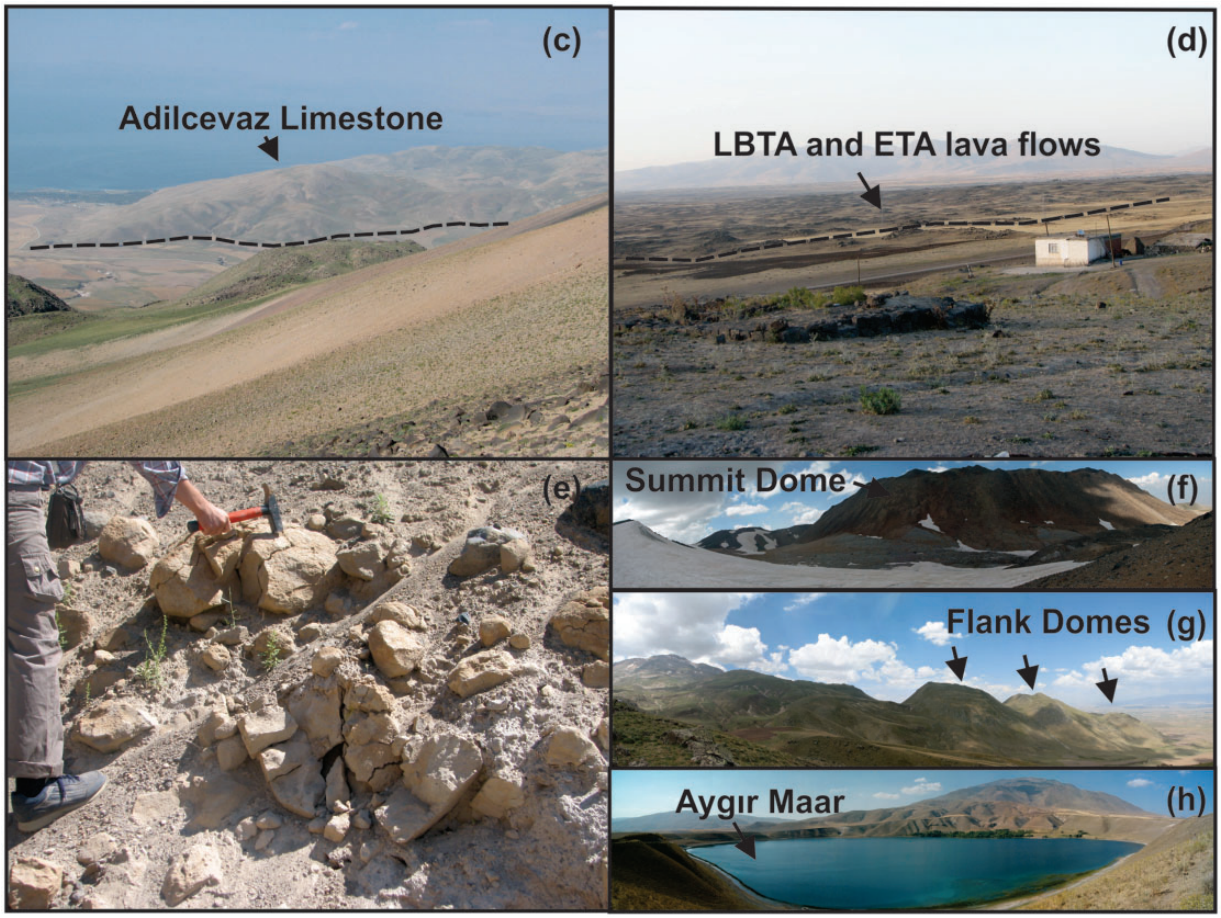


Fig. 1. (continued).

on the Nu system at the PCIGR has been described by Weis *et al.* (2005). During the period of analysis, repeat analysis of international standard NBS 981 yielded $^{206}Pb/^{204}Pb = 16{\cdot}9445 \pm 0{\cdot}0018$ (2σ; $n = 20$), $^{207}Pb/^{204}Pb = 15{\cdot}5017 \pm 0{\cdot}0016$ (2σ; $n = 20$), and $^{208}Pb/^{204}Pb = 36{\cdot}7257 \pm 0{\cdot}0038$ (2σ; $n = 20$). The leached powders of USGS reference material G2 yielded Pb isotopic ratios of $^{206}Pb/^{20}4Pb$, $^{207}Pb/^{204}Pb$ and $^{208}Pb/^{204}Pb$ of $18{\cdot}4019 \pm 0{\cdot}0209$, $15{\cdot}6353 \pm 0{\cdot}0025$ and $38{\cdot}9010 \pm 0{\cdot}0130$, respectively. These values are in agreement with those for leached residues of USGS-G2 from Weis *et al.* (2006).

Ar–Ar age dating of eight samples was performed at the Isotope and Geochronology Laboratories of the University of Nevada. All samples were run as conventional furnace step heating analyses. Samples analyzed by this method utilized a double vacuum resistance furnace similar to the Staudacher *et al.* (1978) design. Sanidine standard 92-176 (Fish Canyon sanidine), with a calibrated age of $28{\cdot}10 \pm 0{\cdot}04$ Ma (Spell & McDougall, 2003), was used as the fluence monitor. Details of the analytical methods and data treatment have been given by Justet & Spell (2001) and Spell & McDougall (2003). The results of eight age determinations (details are given in Supplementary Material 2) are summarized in Table 1.

GEOLOGY, ROCK TYPES AND NEW ^{40}AR–^{39}AR AGES

Süphan is a steep-sided stratovolcano that rises to ~4050 m above the surrounding flatland (~1700 m). Its base diameter is ~40 km. The eruptive products of Süphan extend over an area of about 2000 km^2 (Fig. 1b). Its history has been considered by several researchers within the overall framework of the evolution of the collision-related volcanism in eastern Anatolia (e.g. Innocenti *et al.*, 1976, 1982*a*, 1982*b*; Ercan *et al.*, 1990; Pearce *et al.*, 1990; Notsu *et al.*, 1995; Yılmaz *et al.*, 1998; Keskin, 2003, 2007; Şengör *et al.*, 2008). Previously reported ages for the Süphan volcanic rocks range from 0·1 to 0·7 Ma (e.g. Innocenti *et al.*, 1976; Ercan *et al.*, 1990; Pearce *et al.*, 1990; Notsu *et al.*, 1995; Yılmaz *et al.*, 1998).

Downloaded from https://academic.oup.com/petrology/article-abstract/55/1/37/1524170 by Yuzuncu Yil University user on 23 April 2020

*Table 1: Summary of $^{40}Ar/^{39}Ar$ data for Suphan volcanic rocks**

Sample no.	Rock type	Sample	Total gas age (ka)	Plateau age (ka)	Isochron age (ka)	Coordinates (UTM)
2006 99	Basalt	Plagioclase	934 ± 91	415 ± 103	*428 ± 40*	E308527, N4326028
2007 22	Late BTA	Groundmass	430 ± 36	313 ± 37	*225 ± 29*	E321874, N4299135
2007 24	Late BTA	Groundmass	159 ± 23	195 ± 26	*219 ± 41*	E305400, N4298325
2006 116	Early TA	Groundmass	205 ± 10	162 ± 11	*132 ± 11*	E308850, N4324375
2006 3	Early TA	Groundmass	172 ± 38	405 ± 60	*387 ± 47*	E321500, N4317430
2006 8	Late TA	Groundmass	424 ± 23	381 ± 56	*150 ± 110*	E 31875, N4316625
2006 110	Dacite	Amphibole	–	–	*110 ± 30*	E311875, N4316250
2007 5	Rhyolite	Biotite	310 ± 12	122 ± 19	*64 ± 14*	E312000, N 4311000

*All samples were run as conventional furnace step heating analyses. All data are reported at the 1σ uncertainty level. Preferred ages are shown in italics. BTA; basaltic trachyandesite, TA; trachyandesite.

The volcanic products of Süphan were emplaced over Miocene shallow marine, dolomitized limestones (Adilcevaz Limestone) (Fig. 1c) and Pliocene–Pleistocene fluvial and lacustrine sediments (Fig. 2). Field studies and ^{40}Ar–^{39}Ar age determinations, together with the results of previous studies, have been used to constrain the volcanostratigraphy of Süphan. We summarize the geological evolution of Süphan as follows.

Initial products

Initial products observed around the volcano are mainly silicic in composition and include a debris avalanche, pyroclastic fall deposits and rhyolitic obsidian lava flows (Fig. 2). The debris avalanche deposits are mostly covered by younger units and hence are exposed in only the northern and northeastern parts of the volcano in a few areas. The most characteristic feature of the deposits is their hummocky topography. They are overlain by thin pumice and ash fall deposits and rhyolitic obsidian flows. Ogata *et al.* (1989) reported the K–Ar age of the obsidians as 0·76 ± 0·56 Ma.

Basalt, basaltic trachyandesite and trachyandesite lava flows

Following the rhyolitic obsidian lava flows, an effusive phase which includes a basaltic lava flow and several basaltic trachyandesite and trachyandesite flows began to form the main cone of Süphan. All the products of this effusive phase flowed over the debris avalanche deposits. Our new ^{40}Ar–^{39}Ar isochron age for the basaltic lava is 428 ± 40 ka (Table 1); this is exposed at the northern parts of the volcano (Fig. 2). The basaltic trachyandesite and trachyandesite lavas of Süphan are differentiated as early and late lava flows. Early basaltic trachyandesite lava flows are exposed in limited areas in the southern and northern parts of the study area. Most of the lavas are covered by younger Süphan lavas. Late basaltic trachyandesite lava flows and early trachyandesite flows are mapped as a single lava unit (Figs 1d and 2) as their contact relationship is not well defined in the field. These are the most widespread lava flows in the study area; they include several lava flows, and extend over an area of ~150 km^2 in the western, northern and northeastern parts of the volcano. Our new ^{40}Ar–^{39}Ar isochron ages for the late basaltic trachyandesite lava flows are 225 ± 29 and 219 ± 41 ka (Table 1). The ^{40}Ar–^{39}Ar isochron ages of the early trachyandesite lava flows are in the range 387 ± 47 to 132 ± 11 ka (Table 1). Late trachyandesite lava flows define the current morphology of the stratovolcano and cover an area of ~52 km^2. They are exposed in the southern, northeastern and northern parts of the volcano. Younger pyroclastic deposits of Süphan partly cover these lavas in the southern parts of the volcano. Our new ^{40}Ar–^{39}Ar isochron ages for the late trachyandesite lavas are 150 ± 110 ka (Table 1).

Pyroclastic rocks

The various pyroclastic units of Süphan can be grouped into three phases, each being separated by a paleosol horizon. Phase I pyroclastic rocks start with a green plinian pumice fall deposit (P1-1). The maximum pumice size is up to 2 cm within this unit. P1-1 is lithic-poor, extends radially around the volcano and is overlain by a lithic-rich white plinian pumice fall deposit (P1-2). The pumice and lithic fragments are up to 0·5 and 0·2 cm, respectively, within this unit. A plinian pumice fall deposit (P1-3) with a maximum pumice size of 10 cm overlies the P1-2 unit. It contains large fractured pumice blocks. The broken pieces of the pumice blocks are intact, suggesting that they were deposited before they fractured. Post-deposition fractures indicate that the blocks were still hot when emplaced, then cracked upon cooling. The lithic fragments are up to 3 cm in size. Phase I pyroclastic deposits are terminated by a thin plinian ash fall.

Downloaded from https://academic.oup.com/petrology/article-abstract/55/1/37/1524170 by Yuzuncu Yil University user on 23 April 2020

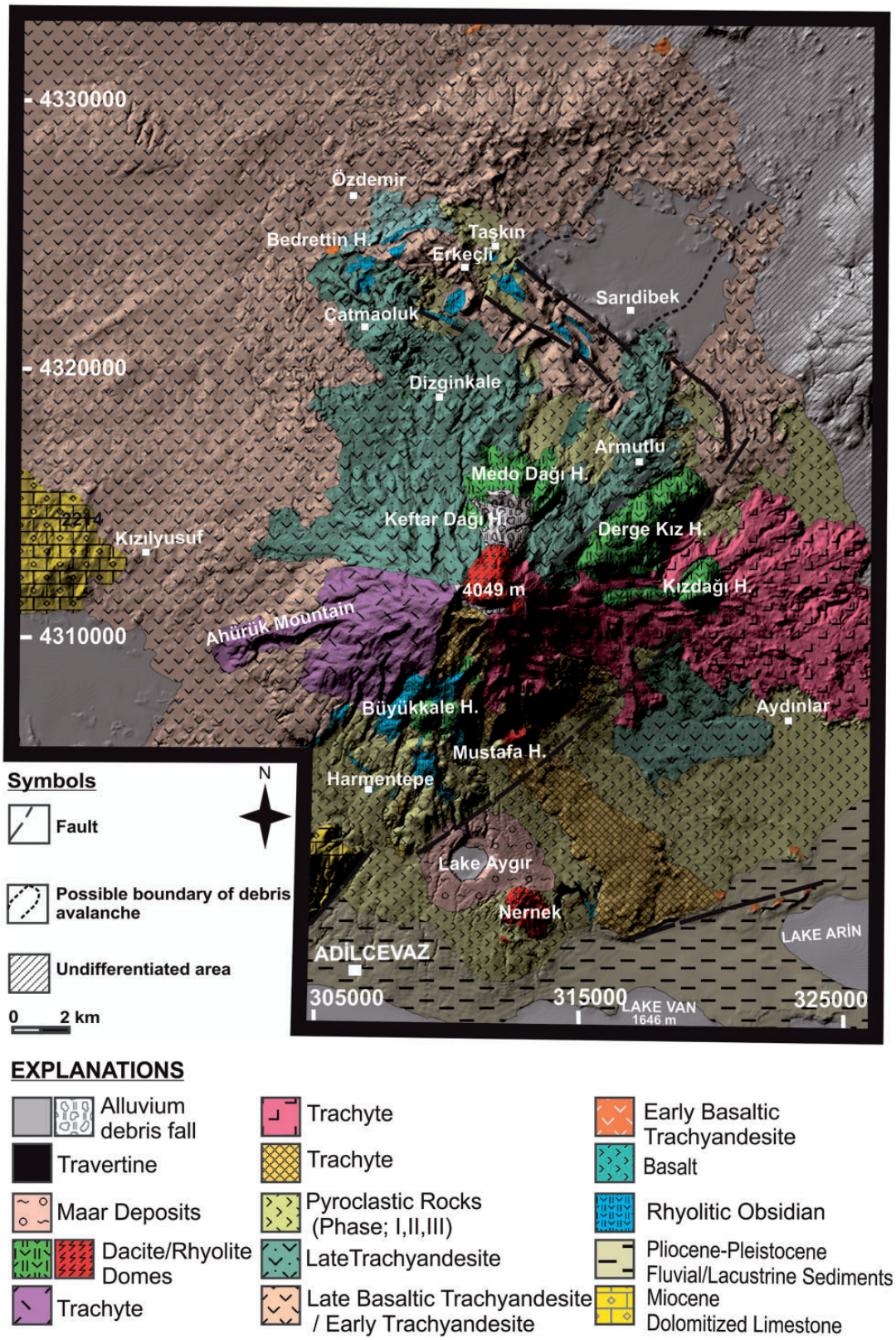


Fig. 2. Geological map of the Süphan stratovolcano.

Downloaded from https://academic.oup.com/petrology/article-abstract/55/1/37/1524170 by Yuzuncu Yil University user on 23 April 2020

Phase II commenced with a block and ash flow. This is one of the most common pyroclastic deposits around Süphan. The size of the blocks is up to 1·5 m in the vicinity of the main cone and gradually decreases away from the volcano. The block and ash flow deposits contain radially fractured blocks (Fig. 1e) and bread-crust bombs, and display reverse grading. White ash fills the spaces between the blocks. The blocks are mostly rhyolitic although rarely fragments of the older deposits of the volcano are present. The block and ash flow deposit is mainly exposed in the southern parts but is also observed in the eastern and northeastern parts of the volcano. This unit seems to have been deposited ~10 km away from the Süphan cone in the southern parts. The block and ash flow deposit is overlain by a thin plinian ash fall deposit.

The last phase of pyroclastic deposits (Phase III) is a white plinian pumice fall deposit (P3-1), characterized by pumice and lithic fragments with maximum sizes of 4 cm and 2 cm, respectively.

Trachyte lava flows

Three trachyte lava flows are recognized on the southern, eastern and western flanks of the volcano. The oldest one has a vitrophyric texture, contains amphibole and covers an area of ~25 km^2 in the southern parts of the volcano. The trachyte in the eastern part extends over an area of 75 km^2 and includes enclaves ranging up to 2 and 7 cm in size. The youngest one is observed on the western flanks and is less glassy than the other trachyte flows, and has a microcrystalline texture.

Dacitic and rhyolitic domes

Dacitic and rhyolitic domes were extruded after the lavas and pyroclastic deposits of the main cone. They are situated at the summit (Fig. 1f) and on the flanks of the volcano (Fig. 1g). They are ellipsoidal to circular and cover an area ranging from 0·25 to 10 km^2. Our new ^{40}Ar–^{39}Ar isochron age for the dacitic dome is 110 ± 30 ka (Table 1). The youngest rhyolitic dome seems to have developed on the summit crater of the volcano. It has a diameter of 1 km and a height of 150 m. This dome possible plugs the main conduit of Süphan volcano. Our new ^{40}Ar–^{39}Ar isochron age for one of the rhyolitic domes is 64 ± 14 ka (Table 1).

Maar deposits

The most recent products of Süphan volcanism are phreatomagmatic in character and associated with a maar, Aygır Maar, which has a circular crater with a diameter of 1·5 km in the southern part of the volcano (Figs 1h and 2). The deposits of the maar extend ~2·5 km away from the crater and show a radial distribution. Base surge deposits from the maar display dune, antidune and cross-bedding structures. Surge deposits are fine grained and poorly sorted. The thickness of the maar deposits at the crater rim is up to 40 m, and decreases away from the maar. The deposits contain (1) ash and grey and white pumice fragments as juvenile fragments, (2) perlite and obsidian fragments as accessory clasts, and (3) sedimentary fragments as accidental clasts. The lower parts of the deposit mostly include accessory clasts and are characterized by large dune and antidune structures.

PETROGRAPHY AND MINERAL CHEMISTRY

The petrography, mineralogy and mineral chemistry of the Süphan lavas have been described in detail by Özdemir *et al.* (2011). Most of the lavas are crystal-rich and porphyritic with a hyalopilitic groundmass. The majority of the phenocryts contain glass and mineral inclusions, and are zoned with reaction rims. Apatite and zircon are found as accessory minerals. Iddingsitization of olivine, and opacitization of amphibole and pyroxene are the major types of alteration observed in some of the lavas (Özdemir *et al.*, 2011).

Olivine phenocrysts are common in basaltic and basaltic trachyandesitic rocks, and are rarely found in trachyandesitic rocks. All crystals are normally zoned with Fo-rich cores. Forsterite contents of olivines are in the range of $Fo_{53–80}$ in basalts, $Fo_{52–71}$ in basaltic trachyandesites, and $Fo_{37–75}$ in trachyandesites (Özdemir *et al.*, 2011). Clinopyroxene is the most common mafic mineral in the basaltic rocks, and decreases in abundance from basalt to dacite. Most phenocrysts are Ca-rich augite and have compositions in the range of $En_{24–45}$, $Fe_{15–33}$, $Wo_{35–44}$. Orthopyroxene is present in the basaltic trachyandesites to rhyolites, with increasing abundance, and ranges from enstatite to ferrosilite, with 1–4 mol % wollastonite component. Plagioclase is the most abundant phenocryst and groundmass phase in all Süphan lavas. It contains abundant inclusions of glass, clinopyroxene, and rarely accessory zircon and apatite. Anorthite contents of plagioclase are in the range $An_{48–59}$ for basalts, $An_{40–54}$ for basaltic trachyandesites, $An_{25–61}$ for trachyandesites, $An_{29–56}$ for trachytes, $An_{26–47}$ for dacites and $An_{9–41}$ for rhyolites. They display normal, reverse and oscillatory zoning in all groups of Süphan lavas and have patchy and sieve textures (Özdemir *et al.*, 2011). K-feldspars are found only in rhyolitic samples and are sanidine in composition (in the range of $An_{1–2}$ and $Or_{61–82}$). Euhedral and subhedral calcic amphibole phenocrysts are found in the trachytes, dacites and rhyolites, and are completely replaced or rimmed by Fe–Ti oxides in the trachytes. Biotite is the most abundant ferromagnesian mineral in the rhyolites and also occurs occasionally in the dacites. Fe–Ti oxides are titanomagnetite and ilmenite, typically occurring as coexisting groundmass crystals and as inclusions in other phenocrysts. They rarely occur as phenocrysts (Özdemir *et al.*, 2011).

Downloaded from https://academic.oup.com/petrology/article-abstract/55/1/37/1524170 by Yuzuncu Yil University user on 23 April 2020

GEOCHEMISTRY

Major and trace element geochemistry

The whole-rock compositions of 60 samples from Süphan were previously reported by Özdemir *et al.* (2011) (Supplementary Material 1). Major element compositions are in the range (on a hydrous basis) of 51·47–74·81 wt % for SiO_2 and 7·15–0·02 wt % for MgO. The Süphan lavas cover a broad compositional spectrum from basalt to rhyolite but cluster in the trachyandesite, trachyte and dacite fields. The majority of the volcanic rocks are subalkaline, although some display transitional characteristics straddling the alkali–subalkali boundary, and a few plot in the alkali field of the total alkalis vs silica diagram (Özdemir *et al.*, 2011). The overall character of the volcanism seems to have changed from mildly alkaline to transitional and subalkaline with time. The transitional and subalkaline products of the volcano are of calc-alkaline and high-K calc-alkaline affinity (Özdemir *et al.*, 2011). Except for a mildly alkaline basaltic lava flow that is slightly nepheline normative, the rest of the volcanic products are hypersthene–quartz normative (Supplementary Material 1).

On conventional Harker diagrams (Fig. 3) Mg-number and CaO/Al_2O_3 decrease with increasing SiO_2 content from mafic to felsic members. Compatible trace elements such as Co, Sc and to a lesser extent Ni (Fig. 3) define negative correlations with SiO_2, indicating that olivine, clinopyroxene and Fe–Ti oxides were important fractionating mineral phases in the petrogenesis of the Süphan lavas. The Sr content of the Süphan lavas decreases from basalt to rhyolite, pointing to an increasing amount of plagioclase fractionation during magmatic differentiation. Incompatible elements such as Ba and Rb increase from mafic to felsic members.

Incompatible trace element characteristics are illustrated as primitive mantle (PM)-normalized element patterns in Fig. 4 and as chondrite-normalized rare earth element (REE) patterns in Fig. 5. As briefly mentioned by Özdemir *et al.* (2011), all rock types (basalt, basaltic trachyandesites, trachyandesites, trachytes, dacites and rhyolites) show similar PM-normalized trace element patterns. In all samples large ion lithophile elements (LILE) are enriched relative to high field strength elements (HFSE). In trachyandesites, the element enrichment level seems to increase from early to late members (Fig. 4). Depletion of Ba, Pb, Sr, P and Ti increases from basalt to rhyolite. The negative Nb and Ta troughs have been suggested to indicate the presence of an inherited subduction component in the mantle source (Özdemir *et al.*, 2011), but could also reflect crustal contamination. The chondrite-normalized REE patterns (Fig. 5) indicate enrichment of light rare earth elements (LREE) over heavy rare earth elements (HREE). The $(La/Yb)_N$ ratio is 3·4 for basaltic rocks and increases slightly with increasing SiO_2: 4·8–5·3 for basaltic trachyandesites, 3·3–5·8 for trachyandesites, 3·6–4·7 for trachytes, 4·6–5·6 for dacites and 5·7–8·0 for rhyolites. The magnitude of the negative Eu anomaly increases with increasing SiO_2. The late trachyandesite lavas (Figs 4 and 5) also have the highest REE contents among all the volcanic rocks, including the high- and low-SiO_2 end-members (Özdemir *et al.*, 2011).

Isotope geochemistry

Sr, Nd and Pb isotopic compositions of selected Süphan volcanic rocks are given in Table 2. $^{87}Sr/^{86}Sr$, $^{143}Nd/^{144}Nd$, $^{208}Pb/^{204}Pb$, $^{207}Pb/^{204}Pb$ and $^{206}Pb/^{204}Pb$ vary in the range 0·703925–0·709579, 0·512520–0·512819, 39·0585–39·4353, 15·6633–15·6943, and 19·0222–19·5497, respectively. The sample with the higher $^{87}Sr/^{86}Sr$ is an older rhyolitic obsidian lava (sample 2005 69). On a $^{87}Sr/^{86}Sr$ vs $^{143}Nd/^{144}Nd$ diagram (Fig. 6a) the mildly alkaline rocks (basalt, early basaltic trachyandesite and early trachyandesite), and a trachyte sample plot close to the Bulk Silicate Earth, whereas the transitional late basaltic trachyandesites, late trachyandesites, dacites and rhyolites have more radiogenic $^{87}Sr/^{86}Sr$ compositions. In Pb–Sr (Fig. 6b) and Pb–Nd (Fig. 6c) isotope diagrams the Süphan volcanic rocks fall between the mantle sources of mid-ocean ridge basalt (MORB) and enriched mantle II (EM II). On Pb–Pb isotope diagrams the volcanic rocks display relatively radiogenic $^{208}Pb/^{204}Pb$, $^{207}Pb/^{204}Pb$ and $^{206}Pb/^{204}Pb$ values (Table 2, Fig. 6d), plotting above the Northern Hemisphere Reference Line (NHRL) and clustering in the EM II and global subducted sediment (GLOSS) fields.

DISCUSSION

Fractional crystallization

To evaluate the differentiation history of the Süphan magmas from mafic to felsic end-members and to determine possible crystallization conditions such as water content and pressure, we use the MELTS code of Ghiorso & Sack (1995). MELTS allows the modeling of liquid lines of descent of silicate magmas as a function of P, T, fO_2 and H_2O. In our modeling we use a basaltic trachyandesitic lava (sample 2006 112) for the starting composition to allow achievement of the composition of the most evolved member of Süphan volcanism. Crystallization temperature interval (~1100°C for sample 2006 112, ~800°C for sample 2005 75) and fO_2 (quartz–fayalite–magnetite; QFM) values are from Özdemir *et al.* (2011). The modeled differentiation trends are compared with the Süphan whole-rock data in Fig. 7. The best match between the modeled and observed differentiation trends was obtained for $P = 2$–4 kbar and $H_2O = 0{\cdot}5$–1 wt %. In Fig. 7, SiO_2-rich late basaltic trachyandesites ($SiO_2 > 53$ wt %, samples 2005 68, 2006 76, 2006 114 and 2006 130, from Özdemir *et al.*, 2011) and late trachyandesites (samples 2006 74, 2005 59, 2006 77, 2006 102, 2006 105 and 2006 8, from Özdemir

Downloaded from https://academic.oup.com/petrology/article-abstract/55/1/37/1524170 by Yuzuncu Yil University user on 23 April 2020

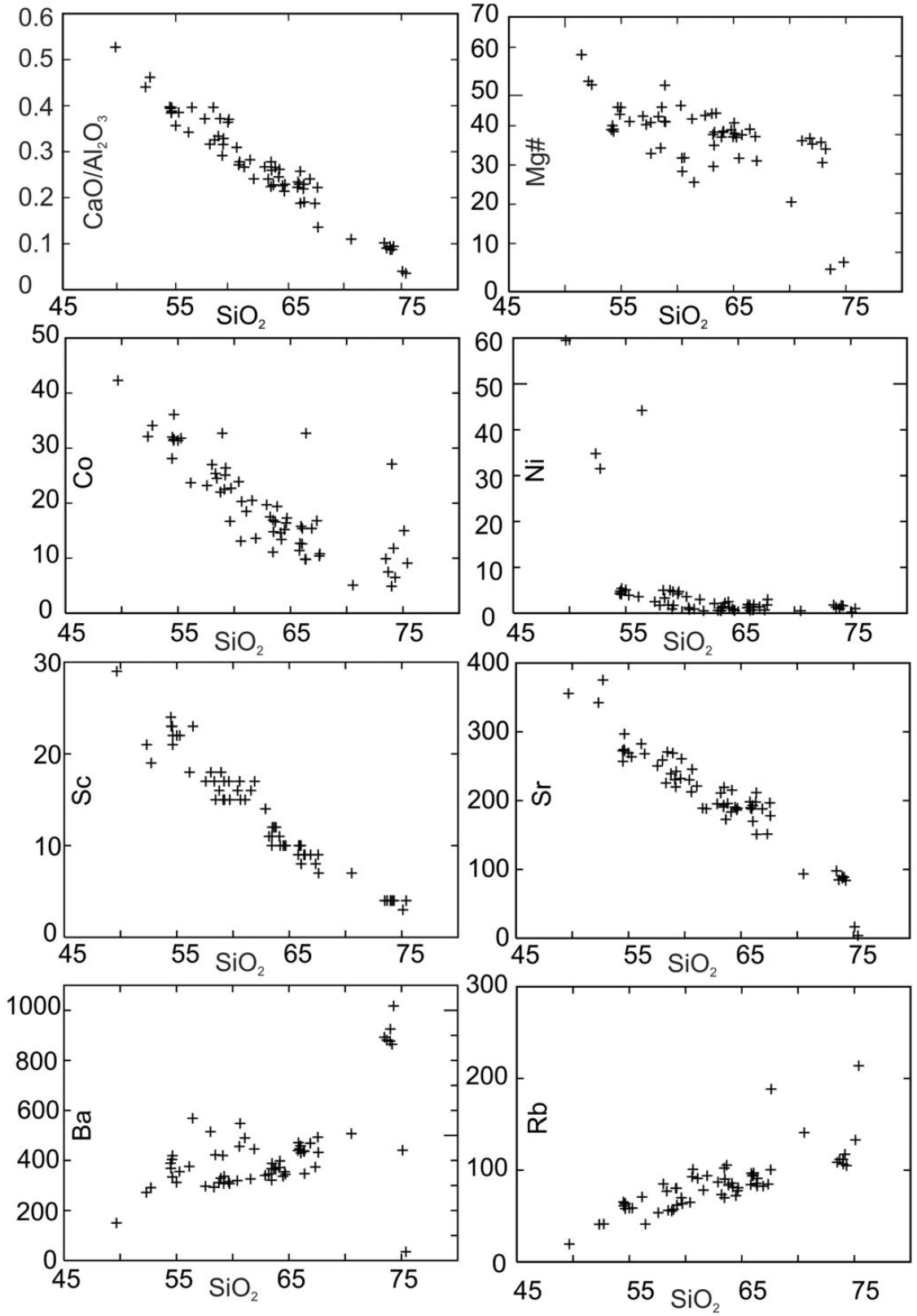


Fig. 3. Variation of CaO/Al_2O_3, Mg# and selected trace elements (ppm) vs wt % SiO_2 for the Süphan volcanic suite.

Downloaded from https://academic.oup.com/petrology/article-abstract/55/1/37/1524170 by Yuzuncu Yil University user on 23 April 2020

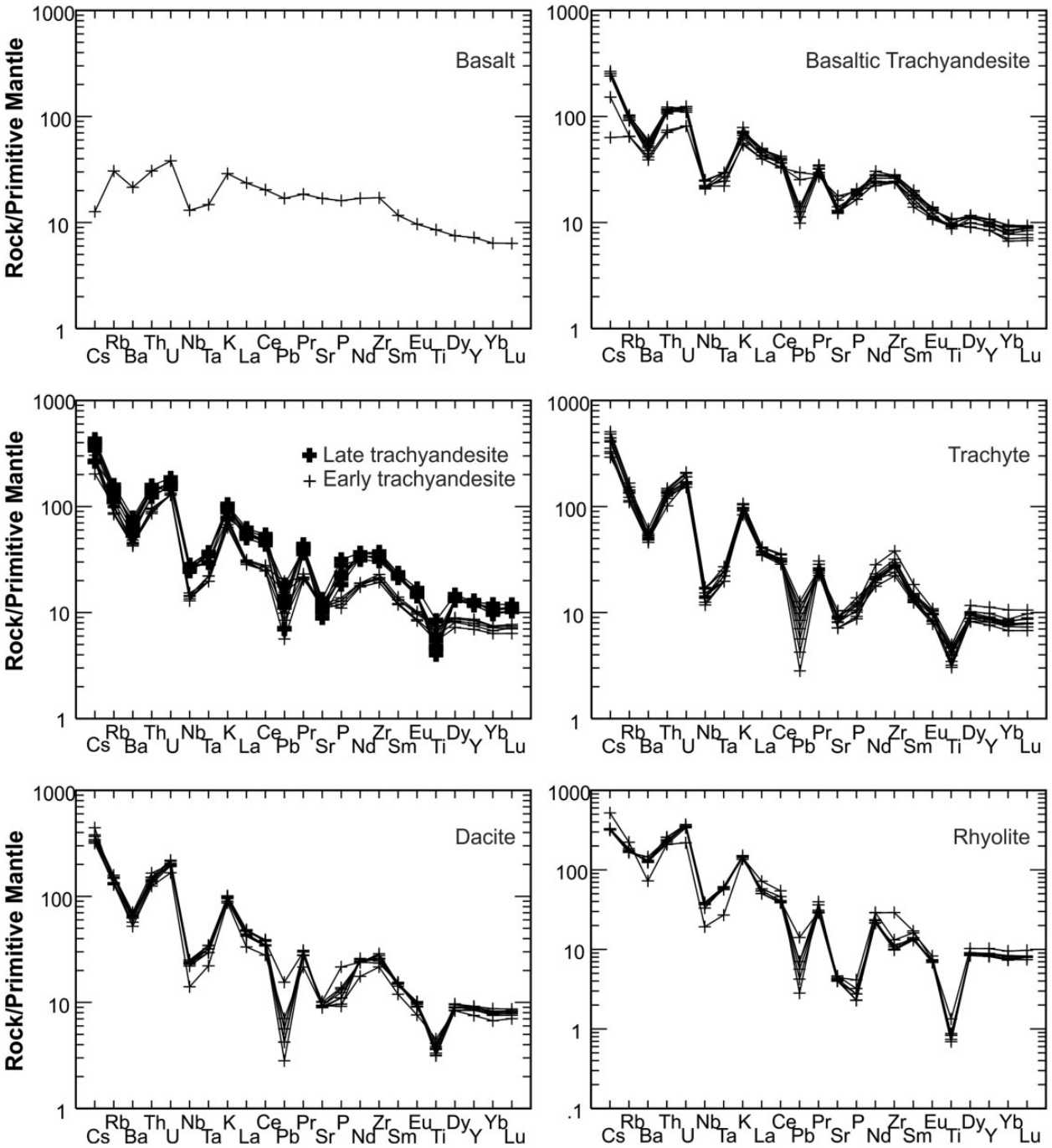


Fig. 4. Primitive mantle normalized incompatible element patterns of the Süphan volcanic rocks. Normalization values are from Sun & McDonough (1989).

et al., 2011) and most of the more evolved members ($SiO_2 > \sim 65$ wt %) of the Süphan volcanic suite plot on the model liquid lines of descent for CaO, MgO and TiO_2. Özdemir *et al.* (2011) obtained similar results by comparing melt inclusion and glass composition data for the Süphan volcanic products with experimentally determined liquid lines of descent for hydrous magmas in different tectonic settings. However, most of the Süphan intermediate lavas with SiO_2 contents between 57 and 65 wt % have higher or lower MgO, CaO and TiO_2 contents at a given SiO_2 content compared with the model MELTS trends. Model fractionating phases obtained from MELTS for an

Downloaded from https://academic.oup.com/petrology/article-abstract/55/1/37/1524170 by Yuzuncu Yil University user on 23 April 2020

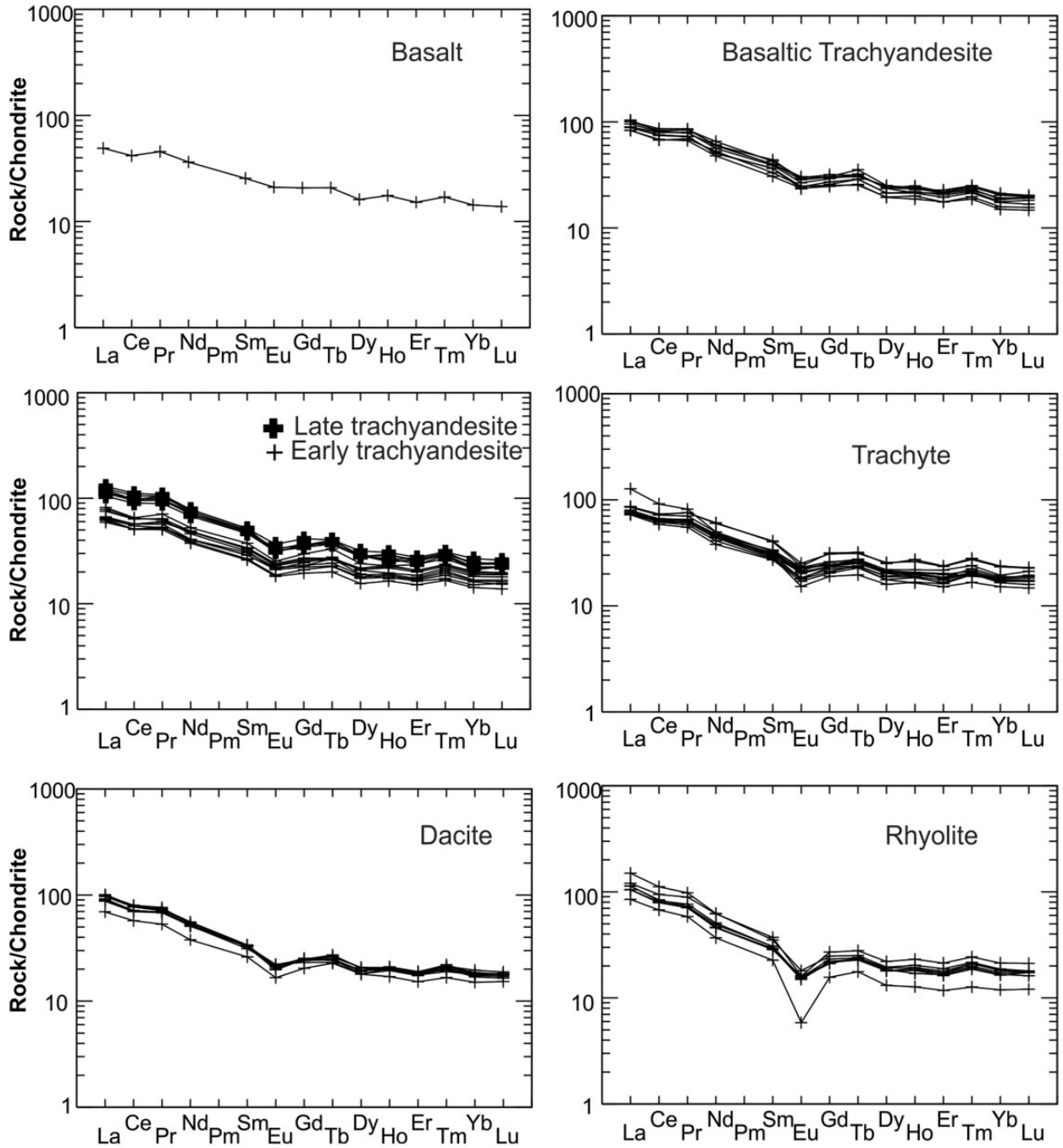


Fig. 5. Chondrite-normalized REE patterns of the Süphan volcanic rocks. Chondrite normalizing values are from Nakamura (1974).

H_2O content of 1 wt % and pressure of 2–4 kbar are similar to the Suphan phenocryst mineralogy. The MELTS modeled fractional crystallization process ($P = 2$ kbar, $fO_2 =$ QFM, $H_2O = 1$ wt %) from the least evolved basaltic trachyandesite (sample 2006 112) to the evolved end-members of the Süphan volcanic suite ($SiO_2 > 65$ wt %) requires ~83% fractional crystallization involving olivine (~2 wt %), clinopyroxene (~12 wt %), orthopyroxene (~5 wt %), plagioclase (~44 wt %), K-feldspar (~10 wt %), spinel (~9 wt %) and apatite (~1 wt %) (Fig. 8a). MELTS modeled crystallization for $P = 4$ kbar and the same fO_2 and water content gives similar mineral compositions and mineral proportions. According to the MELTS modeling olivine crystallizes at high temperature (~1130°C) until 20 wt % of the liquid mass has fractionated. Clinopyroxene, plagioclase, spinel, orthopyroxene,

Downloaded from https://academic.oup.com/petrology/article-abstract/55/1/37/1524170 by Yuzuncu Yil University user on 23 April 2020

Table 2: Isotope compositions of selected Süphan volcanic rocks

Sample no.	Rock type	$^{143}Nd/^{144}Nd \pm 2\sigma$	$^{87}Sr/^{86}Sr \pm 2\sigma$	$^{208}Pb/^{204}Pb \pm 2\sigma$	$^{207}Pb/^{204}Pb \pm 2\sigma$	$^{206}Pb/^{204}Pb \pm 2\sigma$
2006 99	Basalt	0·512819 ± 7	0·703925 ± 7	39·0568 ± 20	15·6628 ± 7	19·0359 ± 9
2005 61	Bas. trachyand.	0·512588 ± 6	0·706199 ± 7	–	–	–
2005 62	Bas. trachyand.	0·512730 ± 7	0·704833 ± 8	39·1542 ± 20	15·6709 ± 7	19·1148 ± 10
2005 68	Bas. trachyand.	0·512785 ± 6	0·706667 ± 8	39·2279 ± 21	15·6943 ± 8	19·0249 ± 9
2006 1	Bas. trachyand.	0·512615 ± 6	0·705939 ± 8	39·2198 ± 22	15·6888 ± 9	19·0245 ± 9
2006 112	Bas. trachyand.	0·512739 ± 8	0·704680 ± 7	39·1258 ± 20	15·6779 ± 9	19·0549 ± 10
2006 114	Bas. trachyand.	0·512577 ± 7	0·706764 ± 9	39·2213 ± 24	15·6932 ± 8	19·0222 ± 10
2005 59	Trachyand.	0·512628 ± 6	0·706446 ± 7	39·2231 ± 23	15·6904 ± 8	19·0626 ± 9
2006 6	Trachyand.	0·512774 ± 6	0·704683 ± 8	39·1234 ± 22	15·6760 ± 8	19·0537 ± 10
2006 8	Trachyand.	–	0·707037 ± 8	39·2594 ± 31	15·6923 ± 9	19·0709 ± 12
2006 72	Trachyand.	0·512773 ± 7	0·704909 ± 8	39·1592 ± 47	15·6693 ± 14	19·1408 ± 19
2006 74	Trachyand.	0·512520 ± 6	0·707180 ± 8	39·2649 ± 21	15·6991 ± 7	19·0296 ± 13
2006 105	Trachyand.	0·512616 ± 10	0·706701 ± 7	39·2400 ± 37	15·6922 ± 14	19·0656 ± 15
2005 10	Trachyte	0·512785 ± 6	0·705012 ± 8	39·1508 ± 18	15·6774 ± 7	19·1164 ± 7
2005 57	Trachyte	–	–	39·1489 ± 18	15·6745 ± 7	19·1281 ± 8
2006 59	Trachyte	0·512766 ± 7	0·704948 ± 8	39·1740 ± 20	15·6732 ± 8	19·1202 ± 9
2007 2	Trachyte	0·512839 ± 6	0·704706 ± 8	39·0929 ± 19	15·6734 ± 8	19·0604 ± 9
2005 28	Dacite	0·512660 ± 6	0·706387 ± 7	–	–	–
2006 110	Dacite	0·512765 ± 6	0·705566 ± 8	39·2433 ± 20	15·6738 ± 7	19·2392 ± 8
2007 4	Dacite	0·512670 ± 8	0·706270 ± 8	39·2622 ± 22	15·6853 ± 7	19·1918 ± 8
2005 69	Rhyolite	0·512691 ± 7	0·709579 ± 8	39·2329 ± 21	15·6766 ± 8	19·1162 ± 8
2007 5	Rhyolite	0·512801 ± 7	0·705238 ± 8	39·4335 ± 24	15·6783 ± 9	19·5498 ± 8
2005 52	Rhyolite	0·512805 ± 6	0·705252 ± 8	–	–	–

apatite and K-feldspar (sanidine) begin to crystallize at 1115, 1110, 1080, 1065, 1020 and 915°C, respectively (Fig. 8b).

Magma mixing

The mismatch between the MELTS modeled fractional crystallization curves and the Süphan whole-rock data between SiO_2 contents of ~57 and ~65 wt % suggests that another process (e.g. magma mixing and/or crustal contamination) may be responsible for the generation of the intermediate members of the volcanic suite. Özdemir *et al.* (2011) proposed that they are the products of mixing between basaltic trachyandesite (~55 wt % SiO_2 at 1100°C) and rhyolite (70–75 wt % SiO_2 at 750°C) magmas, based on the textural complexity of the the phenocrysts in the intermediate lavas, the wide range of calculated temperatures for trachyandesites, trachytes and dacites, and the linear geochemical trends in the intermediate lavas. Here we test the hypothesis that the Süphan intermediate magmas are the result of mixing of basaltic trachyandesitic and rhyolitic melts by using least-squares mixing calculations [Table 3; method of Bryan *et al.* (1969) employed in IGPET software] and the MELTS code of Ghiorso & Sack (1995). The two end-members chosen for the least-squares calculations are basaltic trachyandesites (samples 2005 68 and 2006 112) at ~1100°C and rhyolites (samples 2005 69 and 2005 75) at ~750°C. The SiO_2 contents of the basaltic trachyandesites and rhyolites are in the range of 52·87–55·14% and 75·20–75·47% (on an anhydrous basis), respectively. The blended mixing products are trachyandesites. The least-squares mixing solutions resulted in acceptable values for the sum of squared residuals ($SR^2 < 1$) and give permissive evidence that the intermediate lavas within the Süphan volcanic suite could be related to the mixing of mafic (basaltic trachyandesite) and felsic (rhyolite) end-members.

To better constrain the conditions under which mixing occurred to form the intermediate magmas at Süphan, two of the end-members that were used for least-squares mixing calculations (samples 2006 112 and 2005 69) were used as initial input compositions in the MELTS algorithm to model isobaric–isenthalpic magma mixing. In isobaric–isenthalpic mixing calculations temperature is the dependent variable; so as the pressure stays constant, temperature changes. In our model, 70% of hotter basaltic

Downloaded from https://academic.oup.com/petrology/article-abstract/55/1/37/1524170 by Yuzuncu Yil University user on 23 April 2020

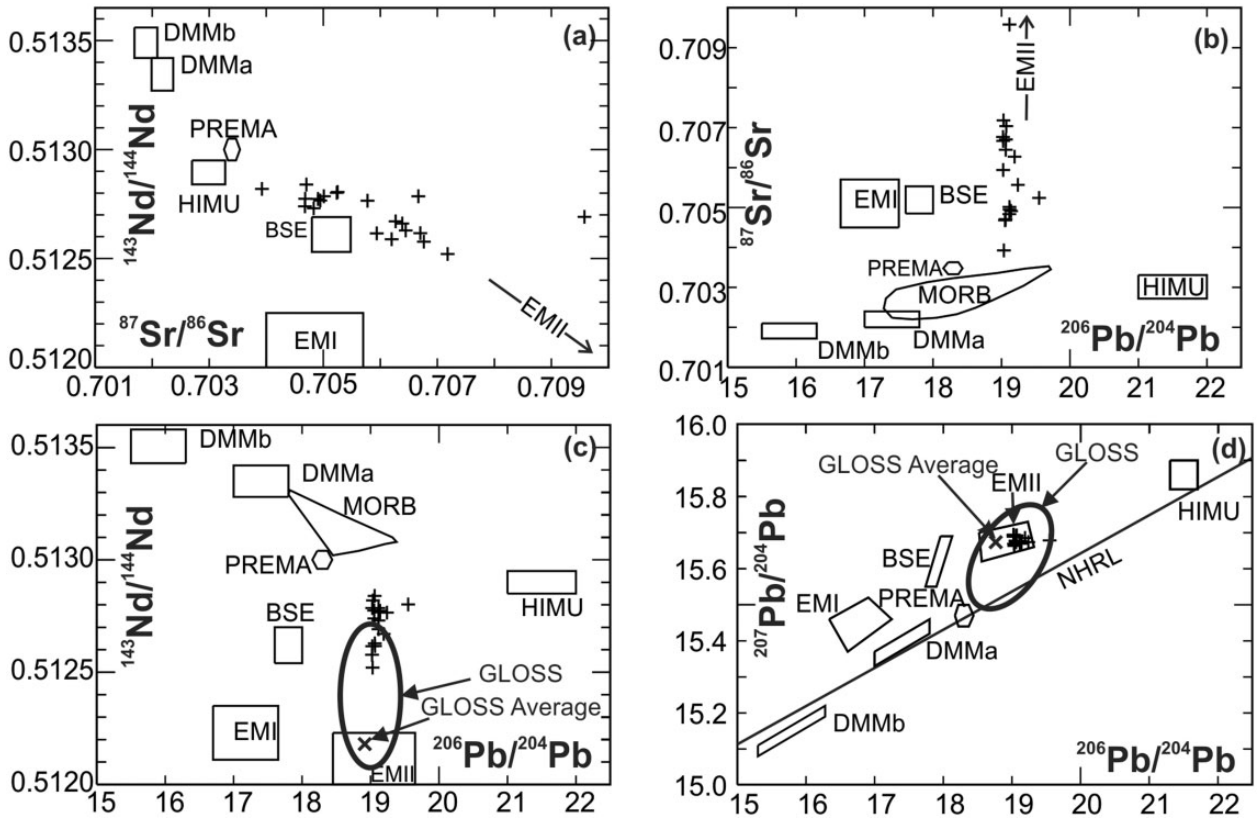


Fig. 6. (a) $^{143}Nd/^{144}Nd$ vs $^{87}Sr/^{86}Sr$, (b) $^{87}Sr/^{86}Sr$ vs $^{206}Pb/^{204}Pb$, (c) $^{143}Nd/^{144}Nd$ vs $^{206}Pb/^{204}Pb$ and (d) $^{207}Pb/^{204}Pb$ vs $^{206}Pb/^{204}Pb$ isotope correlation diagrams for the Süphan volcanic rocks. Global subducted sediments (GLOSS) and GLOSS average are from Plank & Langmuir (1998), The Northern Hemisphere Reference Line (NHRL) is from Hart (1984). Mantle reservoirs are from Zindler & Hart (1986). BSE, Bulk Silicate Earth; DMM, depleted MORB mantle; EM, enriched mantle; HIMU, high μ mantle; PREMA, prevalent mantle.

trachyandesitic magma (at 1100°C; Özdemir *et al.*, 2011) mixes with 30% of cooler rhyolitic magma (at 900°C; Özdemir *et al.*, 2011) under isobaric–isenthalpic conditions. To obtain better results we used various crustal pressures between 0·5 and 1·5 kbar; the best fit was obtained for 0·5 kbar. The results of isobaric–isenthalpic mixing are illustrated in MgO vs SiO_2 and CaO vs SiO_2 plots in Fig. 9. The good agreement between the calculated melt compositions and the Süphan intermediate rock compositions supports the argument that low-pressure isobaric–isenthalpic magma mixing is the controlling process for the chemical diversity of the Süphan intermediate members. In addition to conventional mixing between contrasted melts, the study of Özdemir *et al.* (2011) shows that some mixing also occurred between evolved melts and crystals from ancestral plutonic residues, based on the presence of gabbroic crystal clots in the Süphan lavas.

MELTS fractional crystallization and mixing models reveal that chemical differentiation from a hydrous prental mafic magma occurred at a pressure of 2–4 kbar beneath Süphan and that mixing took place at somewhat shallower levels (0·5 kbar). Özdemir *et al.* (2011) reported similar results, based on melt inclusion data of the Süphan volcanic rocks. They proposed a two-stage petrogenetic model for Süphan volcanism based on mineral and melt inclusion geochemistry. Mantle-derived hydrous basalt stalls in the lower to mid-crust, whereupon it crystallizes to produce more evolved melts. A variety of evolved melts then ascend to shallow crustal levels where they interact.

Crustal contamination

Although the major element trends can be reproduced by fractional crystallization and magma mixing, the large ranges of Sr–Nd isotopic compositions suggest additional contributions from lower and/or upper crustal sources. Süphan volcanic rocks display two distinct trends in $^{87}Sr/^{86}Sr$ vs SiO_2 (Fig. 10a) and $^{143}Nd/^{144}Nd$ vs SiO_2 diagrams (Fig. 10b). However, no covariation is observed between $^{208}Pb/^{204}Pb$, $^{206}Pb/^{204}Pb$ and SiO_2 (not shown). These observations suggest that the Süphan magmas have been contaminated by a component with high $^{87}Sr/^{86}Sr$ and low $^{143}Nd/^{144}Nd$. A plausible contaminant would be the upper crust that has interacted with the Süphan magmas during their ascent or in subvolcanic magma

Downloaded from https://academic.oup.com/petrology/article-abstract/55/1/37/1524170 by Yuzuncu Yil University user on 23 April 2020

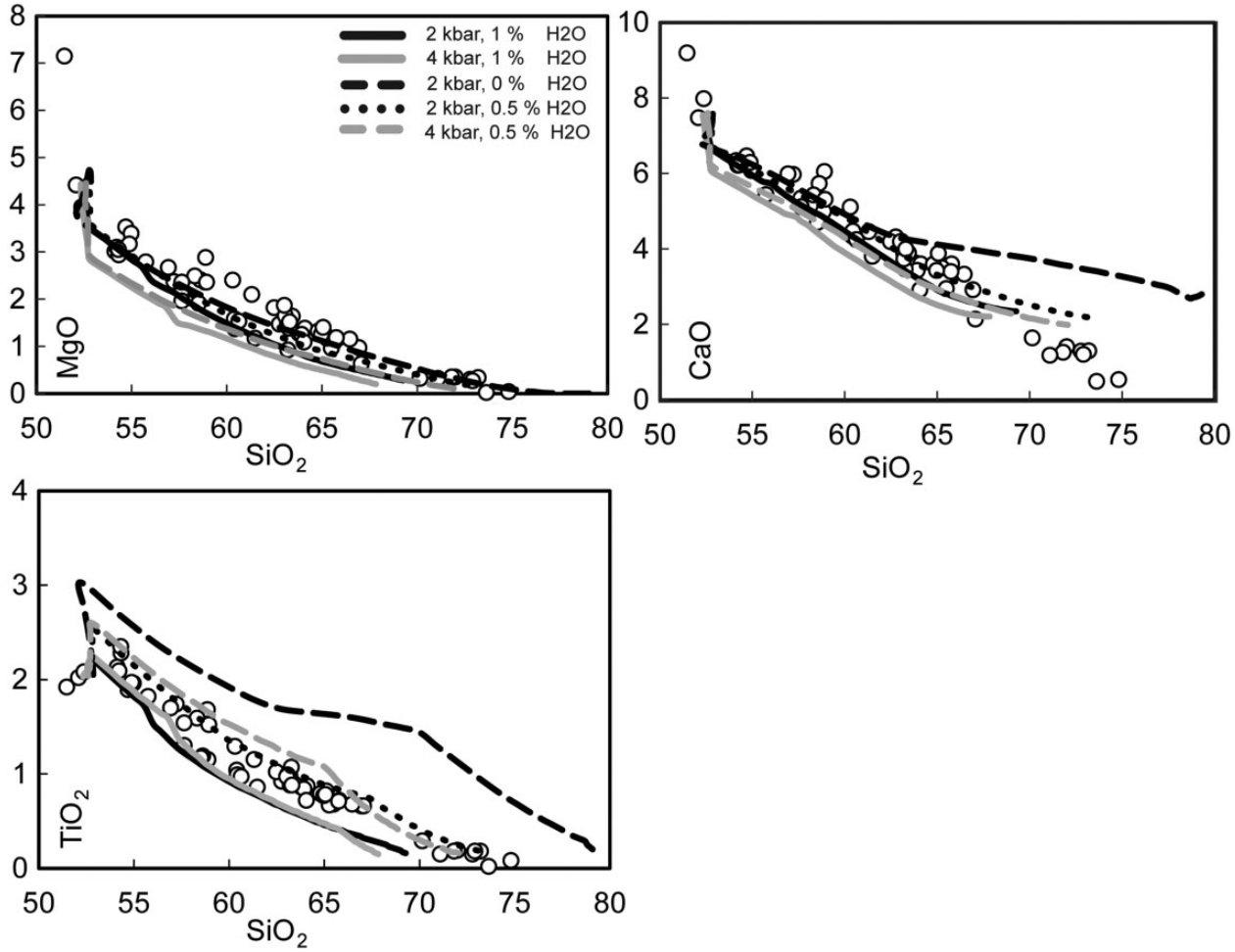


Fig. 7. Variation of MgO, CaO and TiO_2 vs SiO_2 for the Süphan volcanic rocks compared with MELTS (Ghiorso & Sack, 1995) fractional crystallization modeling curves. Crystallization temperature interval (~1100°C for sample 2006 112, ~800°C for sample 2005 75) and fO_2 (QFM) values are from Özdemir *et al.* (2011). Calculation parameters: 2 kbar hydrous (1% H_2O) (black continuous curve), 2 kbar hydrous (0·5% H_2O) (black dotted curve), 2 kbar anhydrous (black dashed curve), 4 kbar hydrous (1% H_2O) (grey continuous curve), 4 kbar hydrous (0·5% H_2O) (grey dashed curve).

chambers. Lavas that seem to be highly contaminated by a component with more radiogenic ^{87}Sr are mostly late basaltic trachyandesites (samples 2005 61, 2005 68, 2006 1 and 2006 114), late trachyandesites (samples 2005 59, 2006 8, 2006 74 and 2006 105) and some of the dacitic and rhyolitic lavas (i.e. samples 2005 28, 2007 4 and 2005 69). These seem to have originated from fractional crystallization of a mafic parental magma (i.e. samples plotting along the MELTS modeled trends in Fig. 7). This requires simultaneous occurrence of fractional crystallization and assimilation of upper crustal rocks. Lavas that seem to be slightly contaminated by upper crustal lithologies are mostly those that appear to be the products of mixing between mafic and felsic end-members (i.e. samples plotting along the MELTS modeled trends in Fig. 9). On this basis, bulk mixing, assimilation and fractional crystallization (AFC) calculations were undertaken to test these observations using the standard upper crust compositions of Bohrson & Spera (2001) (Fig. 10c). The starting composition for AFC modeling is the most mafic member of the Süphan volcanic suite that has the most unradiogenic Sr isotope composition (sample 2006 99). A simple mixing curve between the upper crust and sample 2006 99 is completely different from the Süphan volcanic array. However, AFC (De Paolo, 1981) (Fig. 10c) trajectories can accommodate some of the data. The samples that plot between curves for different r (the ratio of assimilation rate to crystallization rate) values are those that were inferred to have originated mostly by fractional crystallization in Fig. 7 and plot within the field enclosed by dashed lines in Fig. 10a and b. In Fig. 10c we also test the hypothesis that the Süphan intermediate magmas are the products of mixing between mafic and felsic end-members. A number of the samples in Fig. 10c can be reproduced by bulk mixing between

Downloaded from https://academic.oup.com/petrology/article-abstract/55/1/37/1524170 by Yuzuncu Yil University user on 23 April 2020

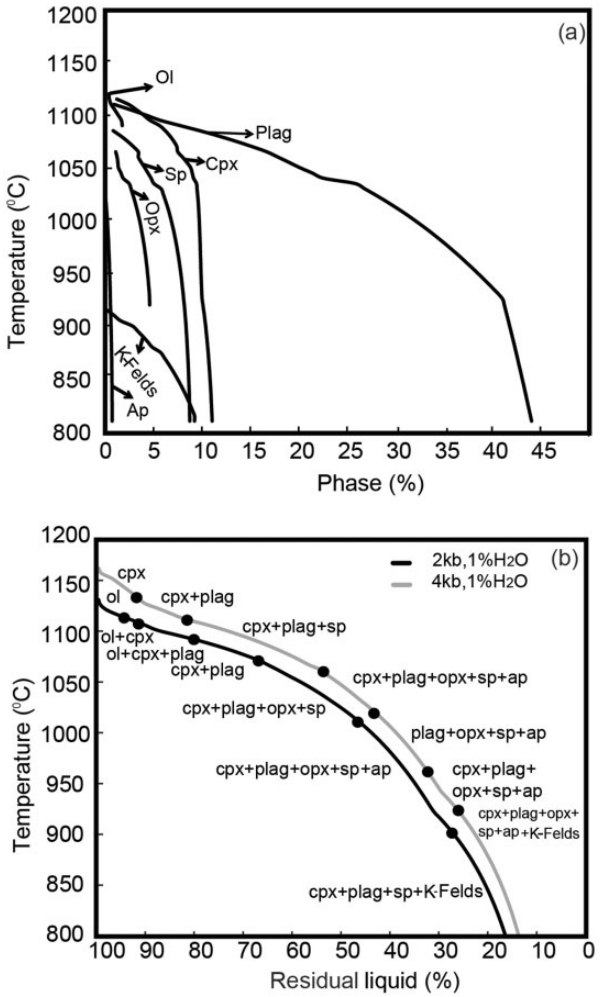


Fig. 8. (a) Proportions of crystallized phases obtained from MELTS with $P = 2$ kbar, fO_2 = QFM, $H_2O = 1$ wt %. (b) Liquidus temperatures (°C) and fractionating mineral assemblages calculated with MELTS for residual liquid percentage from the starting composition sample 2006 112 (Supplementary Data Table 1). ol, olivine; opx, orthopyroxene; cpx, clinopyroxene; plag, plagioclase; sp, spinel; ap, apatite; K-felds, K-feldspar.

sample 2006 112 and sample 2005 69. To evaluate better the role of crustal assimilation we also used the energy-constrained assimilation and fractional crystallization (EC-AFC) model of Bohrson & Spera (2001) and Spera & Bohrson (2001) to model the variation of $^{87}Sr/^{86}Sr$ vs Sr and $^{87}Sr/^{86}Sr$ vs $^{143}Nd/^{144}$ Nd. The EC-AFC model tracks the system as the magma cools and crystallizes and the wall-rock heats up and partially melts. The thermal and compositional parameters of the EC-AFC calculation for the Süphan volcanic uites are given in Table 4. The thermal parameters are those used by Bohrson & Spera (2001) for standard upper and lower crust. Because there are virtually no data for the chemical or isotopic composition of the basement rocks in eastern Anatolia, the compositional parameters for the assimilants are also taken from Bohrson & Spera (2001), although it is difficult to assess the appropriateness of these assigned values. Sample 2006 99 was taken as the starting magma because of its mafic composition (mg# 60) and low $^{87}Sr/^{86}Sr$ and high $^{143}Nd/^{144}Nd$. The results of the EC-AFC modeling are illustrated in Fig. 11a and b. On the $^{87}Sr/^{86}Sr$ vs Sr plot, both upper and lower crustal EC-AFC curves are shown. The Süphan volcanic rocks seem to be most consistent with the curve for upper crustal contamination, rather than lower crustal contamination, with a liquidus temperature, solidus temperature and initial temperature of 1000°C, 900°C and 300°C, respectively. The model indicates that the amount of crustal contamination ranges from ~2 to 10%. It should be noted here that for a less radiogenic crust ($^{87}Sr/^{86}Sr < 0{\cdot}722$), the amount of crustal contamination would increase. The lack of isotopic data for eastern Anatolian basement rocks prevents a better estimate.

Magma generation and partial melting processes

To establish the nature of the mantle source of the Süphan parental magmas, partial melting models using rare earth element (REE) ratios have been constructed to determine the conditions of partial melting along with the mineralogy and chemistry of the source using the method of Shaw (1970). We have used REE ratios that are useful for determining of the extent and depth of partial melting. Partial melting of either a garnet or spinel peridotite source will enrich the light REE (LREE) content (e.g. La) in the melt and produce La/Yb variations with variable degrees of partial melting. Garnet-facies melts will have higher La/Yb ratios relative to spinel-facies melts (Shaw *et al.*, 2003; Peters *et al.*, 2008). Enrichment of middle REE (MREE; e.g. Dy) relative to the heavy REE (HREE; e.g. Yb) depends on whether garnet exists as a residual phase during melting, as the HREE are preferentially retained by garnet during melting (high $D_{Yb} \sim 4{\cdot}0$–15) relative to MREE ($Dy \sim 1{\cdot}0$–$4{\cdot}0$) (Shaw *et al.*, 2003; Peters *et al.*, 2008). Thus, Dy/Yb ratios increase with decreasing degree of partial melting in the garnet facies. However, melting of a spinel peridotite will result in minimal variation in Dy/Yb ratios. Figure 12 shows the variation of $(Dy/Yb)_N$ vs $(La/Yb)_N$, and Yb vs La/Yb for the Süphan volcanic suite, along with trajectories for non-modal batch melting of garnet and spinel peridotite sources.

To minimize the effects of AFC processes, we have extrapolated the concentrations of all major and trace elements back to 7 wt % MgO by fitting linear least-squares regression lines to the Süphan data arrays and using the slopes of the regressed lines to correct the data (see Klein & Langmuir, 1987; Turner & Hawkesworth, 1995). A fractionation correction process was applied to all the trace element compositions of the more mafic lavas (MgO

Downloaded from https://academic.oup.com/petrology/article-abstract/55/1/37/1524170 by Yuzuncu Yil University user on 23 April 2020

Table 3: Least-squares mixing results for selected Süphan volcanic rocks (H_2O-free)

	Test 1				Test 2			
	Basaltic trachyand. end-member 2006 112	Rhyolitic end-member 2007 95	Observed trachyand. 2006 95	Calculated trachyand.	Basaltic trachyand. end-member 2005 68	Rhyolitic end-member 2007 75	Observed trachyand. 2006 86	Calculated trachyand.
SiO_2	52·87	75·47	60·08	59·99	55·14	75·47	59·72	59·87
TiO_2	2·05	0·02	1·22	1·42	2·39	0·02	1·7	1·83
Al_2O_3	17·2	14·08	16·15	16·24	16·01	14·08	16·04	15·55
Fe_2O_3	9·11	0·86	6·75	6·53	10·3	0·86	7·58	8·09
MnO	0·14	0·07	0·13	0·12	0·18	0·07	0·13	0·16
MgO	4·49	0·02	2·47	3·09	3·1	0·02	2·39	2·38
CaO	7·58	0·5	5·87	5·37	6·32	0·5	5·06	4·95
Na_2O	4·42	4·34	4·44	4·39	4·05	4·34	4·61	4·12
K_2O	1·7	4·6	2·57	2·61	2·1	4·6	2·48	2·69
P_2O_5	0·45	0·03	0·31	0·32	0·42	0·03	0·28	0·33
% Basaltic trachyandesite	68·7				76·6			
% Rhyolite	31·3				23·4			
SR^2	0·75				0·83			

	Test 3			
	Basaltic trachyand. end-member 2006 11	Rhyolitic end-member 2005 69	Observed trachyand. 2005 60	Calculated trachyand.
SiO_2	52·87	75·2	62·04	61·94
TiO_2	2·05	0·08	1·16	1·26
Al_2O_3	17·2	13·59	15·98	15·76
Fe_2O_3	9·11	1·28	6·56	5·95
MnO	0·14	0·03	0·13	0·1
MgO	4·49	0·04	2·13	2·7
CaO	7·58	0·54	4·51	4·75
Na_2O	4·42	4·27	4·49	4·36
K_2O	1·7	4·94	2·68	3·01
P_2O_5	0·45	0·03	0·31	0·28
% Basaltic trachyandesite	59·7			
% Rhyolite	40·3			
SR^2	0·93			

SR^2: sum of squared residuals

>2·9 wt %). The corrected La, Yb and Dy concentrations of the Süphan volcanic rocks are plotted in Fig. 12. The slopes, intercepts and r^2 values for all regressions against MgO are given in Table 5. Despite the fact that 7 wt % MgO is too low for the calculated compositions to be representative of primary magmas, this value is appropriate for correcting the majority of the fractionation effects. Given that crustal assimilation is likely to accompany the fractionation

Downloaded from https://academic.oup.com/petrology/article-abstract/55/1/37/1524170 by Yuzuncu Yil University user on 23 April 2020

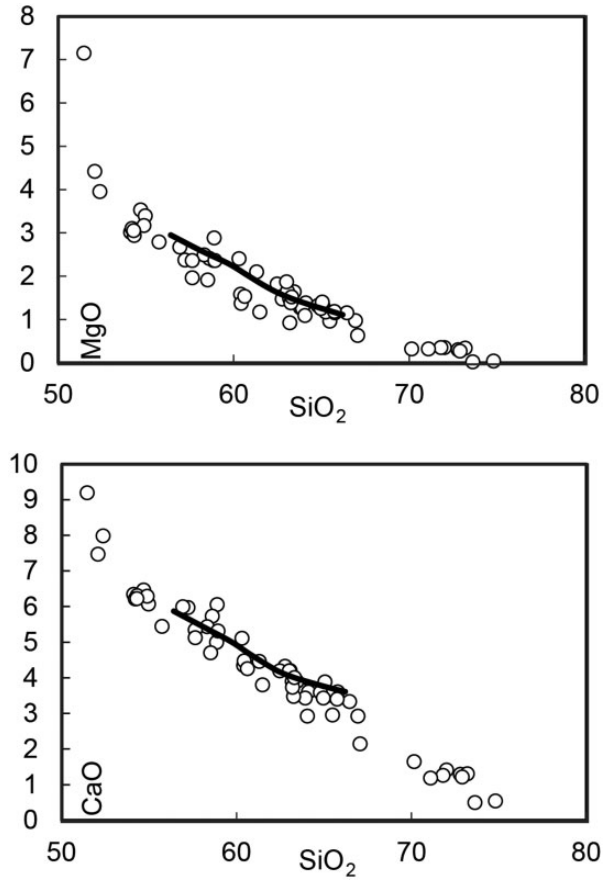


Fig. 9. Variation of CaO and MgO vs SiO_2 (wt %) for Süphan volcanic rocks and MELTS (Ghiorso & Sack, 1995) isobaric–isenthalpic mixing curves. Continuous curves are the result of isobaric–isenthalpic mixing of 70% basaltic trachyandesite (at 1100°C) with 30% rhyolitic magma (at 900°C) at 0·5 kbar. Magma compositions (Supplementary Material 1) and temperatures are from Özdemir *et al.* (2011). (See text for details.)

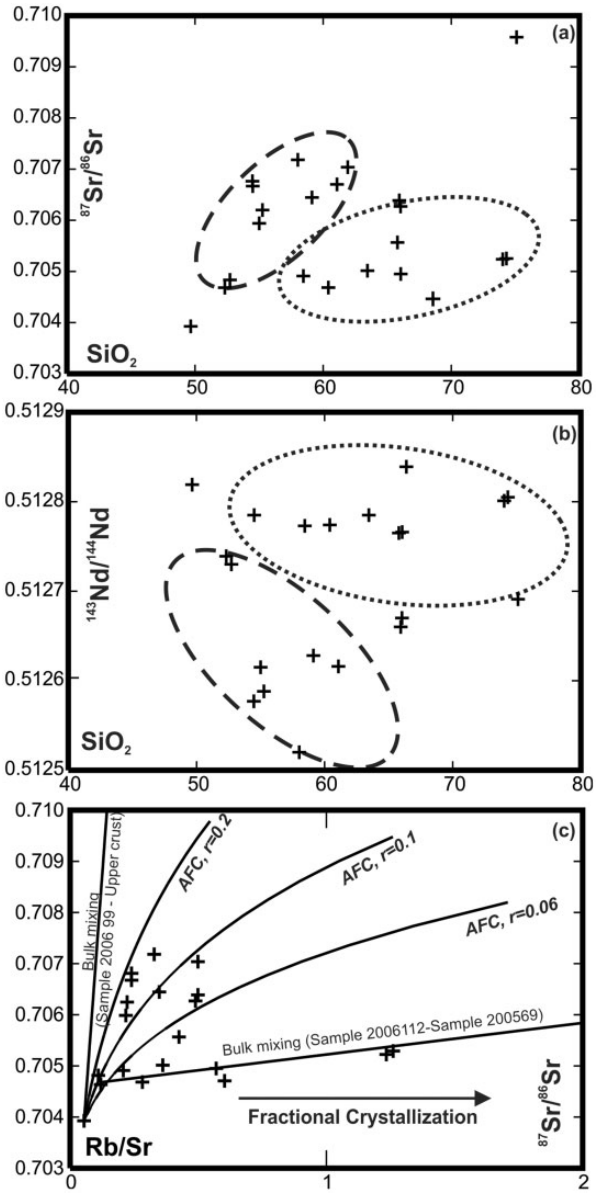


Fig. 10. (a) $^{87}Sr/^{86}Sr$ vs SiO_2 and (b) $^{143}Nd/^{144}Nd$ vs SiO_2 for Süphan volcanic rocks. The field enclosed by dashed lines encompasses the samples that are compatible with fractional crystallization of a mafic magma (i.e. samples plotting along the MELTS modeled trends in Fig. 7). Dotted lines enclose the field that encompasses the samples that are the products of mixing between mafic and felsic end-members (i.e. samples plotting along the MELTS modeled trends in Fig. 9). (c) $^{87}Sr/^{86}Sr$ vs Rb/Sr highlighting the effects of assimilation–fractional crystallization (AFC, DePaolo, 1981) processes in the Süphan volcanic suite. Bulk distribution coefficients are calculated using the modal mineralogy composition of sample 2006 99 ($Plagioclase_{0·5} + Clinopyroxene_{0·3} + Olivine_{0·18} + Ilmenite_{0·02}$). Partition coefficients of the elements used for AFC modelling are from Geochemical Earth Reference Model home page (http://www.earthref.org); the average upper crustal composition is from Bohrson & Spera (2001). *r* values represent the ratio of assimilation rate to crystallization rate. Bulk mixing lines are also shown between sample 2006 99 (average upper crust) and sample 2006 112–sample 2005 69 (see text for details).

processes, extrapolation to 7 wt % MgO also removes the majority of the crustal contamination effects. Only samples with MgO >2·9 wt % were used, to minimize errors resulting from over-extrapolation.

Because of the absence of mantle xenoliths from eastern Anatolian volcanic rocks, we used a primitive mantle source composition as a crude approximation to begin the modeling calculations. Element concentrations in primitive mantle, partition coefficients and mineral assemblages in spinel and garnet peridotites are from McKenzie & O'Nions (1991). Mineral proportions incorporated into the non-modal batch melts are from Thirlwall *et al.* (1994), Shaw *et al.* (2003), Peters *et al.* (2008). In Fig. 12a and b, only mafic samples (MgO >2·9 wt %; i.e. basaltic and basaltic trachyandesitic lavas) are shown. The model results indicate that melting of garnet- or spinel-facies mantle could not alone reproduce the Süphan mafic rocks. To test the contribution of both spinel- and garnet-facies mantle in the

Downloaded from https://academic.oup.com/petrology/article-abstract/55/1/37/1524170 by Yuzuncu Yil University user on 23 April 2020

*Table 4: EC-AFC parameters for the Süphan volcanic rocks and potential contaminants (lower and upper crust)**

Thermal parameters	Upper crust	Lower crust
Magma liquidus temperature (°C)	1280	1320
Magma initial temperature (°C)	1280	1320
Assimilant liquidus temperature (°C)	1000	1100
Assimilant initial temperature (°C)	300	600
Solidus temperature (°C)	900	950
Equilibration temperature (°C)	980	980
Crystallization enthalpy ($J kg^{-1}$)	39 600	39 600
Isobaric specific heat of magma ($J kg^{-1} K^{-1}$)	1484	1484
Fusion enthalpy ($J kg^{-1}$)	270 000	350 000
Isobaric specific heat of assimilant ($J kg^{-1} K^{-1}$)	1370	1388
Compositional parameters, Sample 2006 99	**Sr**	**Nd**
Magma initial concentration (ppm)	356	23
Magma isotope ratio	0·70392	0·512819
Magma trace element distribution coefficient	1·5	0·09
Assimilant (upper crust)		
Assimilant initial concentration (ppm)	350	26
Assimilant isotope ratio	0·722	0·5118
Assimilant trace element distribution coefficient	1·5	0·25
Assimilant (lower crust)		
Assimilant initial concentration (ppm)	230	12·7
Assimilant isotope ratio	0·71	0·513
Assimilant trace element distribution coefficient	0·05	0·25

*The thermal and compositional parameters for standard upper and lower crust are from Bohrson & Spera (2001). (See text for details.)

petrogenesis of the Süphan volcanic rocks, two-component mixing lines or curves (Langmuir *et al.*, 1978) are shown. All the samples plot between mixing lines for melts derived by 2% (Fig. 12a) and 2–5% (Fig. 12b) melting of garnet- and spinel-facies mantle. The contribution of the garnet- and spinel-facies mantle in the genesis of the magmas corresponds to a garnet/spinel peridotite ratio of between 40/60 and 60/40 in Fig. 12.

Subduction components

A key feature of the Süphan volcanic rocks is the LILE enrichment and the presence of negative HFSE (Nb and Ta in particular) anomalies in their trace element patterns (Fig. 4), suggesting similarities with magmas generated in subduction-related tectonic settings. The presence of a subduction component in the source region of the Süphan parental magmas is related to the northward subduction of multiple branches of the Neo-Tethys Ocean under the southern margin of Eurasia since Mesozoic times. Based on previous studies, subduction-related metasomatic components can be broadly classified as (1) fluids from altered oceanic crust (Tatsumi *et al.*, 1986; Hawkesworth *et al.*, 1993, 1997; Turner *et al.*, 1996; Turner, 2002; Guo *et al.*, 2005) or subducted sediments (Ryan *et al.*, 1995; Class *et al.*, 2000; Elburg *et al.*, 2002) or (2) partial melts of subducted sediments or the oceanic crust itself (e.g. Hawkesworth *et al.*, 1993, 1997; Elliott *et al.*, 1997; Elburg *et al.*, 2002; Guo *et al.*, 2005). It has been shown that some LILE (e.g. Rb, Ba, Sr, U) are mobile in aqueous fluids because these elements are water soluble; however, the REE and HFSE (e.g. Ce, Th, Nb, Zr and Ta) are less mobile or immobile in a fluid phase (Sheppard & Taylor, 1992; Turner *et al.*, 1997; Elburg *et al.*, 2002; Turner, 2002). These characteristics lead to high concentrations of some water-soluble LILE and other fluid-mobile elements (e.g. Rb, Ba), and very low contents of HFSE in subduction-derived fluids. Thus, those magmas whose source was strongly metasomatized by a fluid component are likely to have higher Ba/Th (>170; Hawkesworth *et al.*, 1997), Pb/Ce (>0·1; Elburg *et al.*, 2002) and Ba/La ratios than magmas whose source was enriched by partial melts of oceanic crust and subducted sediments (Sheppard & Taylor, 1992; Elburg *et al.*, 2002). In contrast, arc volcanic rocks with a strong imprint of a subduction-related partial melt or subducted sediment in their source region have higher Th/Ce (>0·15; Hawkesworth *et al.*, 1997), $^{87}Sr/^{86}Sr$, $^{206}Pb/^{204}Pb$ (Hawkesworth *et al.*, 1997; Guo *et al.*, 2005, 2006) and lower Ba/La (Sheppard & Taylor, 1992) than those related to fluid metasomatism of their mantle source. Both fluid- and melt- (or bulk subducted sediment) related metasomatism could be responsible for the negative Nb–Ta anomalies of the Süphan volcanic rocks. All of the Süphan mafic volcanic rocks have low Ba/Th (<170) ratios, similar to the global subducting sediment composition (GLOSS; Plank & Langmuir 1998; Fig. 13a). Pb/Ce (<0·1), Ba/La (Fig. 13b) and Th/Ce (most samples >0·5) ratios suggest that the mantle source of the Süphan parental magmas was modified by bulk sediment or a partial melt of subducted sediment rather than by fluids from subducted oceanic crust or subducted sediments. The involvement of subducted sediments in the mantle source has also been proposed by Mutlu *et al.* (2012) based on the $CO_2/^3He$ ratios of the gas phases associated with the geothermal fluids of eastern Anatolia. $^{206}Pb/^{204}Pb$, $^{207}Pb/^{204}Pb$ and $^{208}Pb/^{204}Pb$ isotopic ratios further support a sediment contribution to the mantle source of the Süphan magmas. The higher Pb isotopic ratios of Süphan overlap with the GLOSS and EM II components (Fig. 6c and d). GLOSS is dominated by terrigenous material and therefore similar to the upper continental crust in composition (Plank & Langmuir, 1998). The EM II component has been variously

Downloaded from https://academic.oup.com/petrology/article-abstract/55/1/37/1524170 by Yuzuncu Yil University user on 23 April 2020

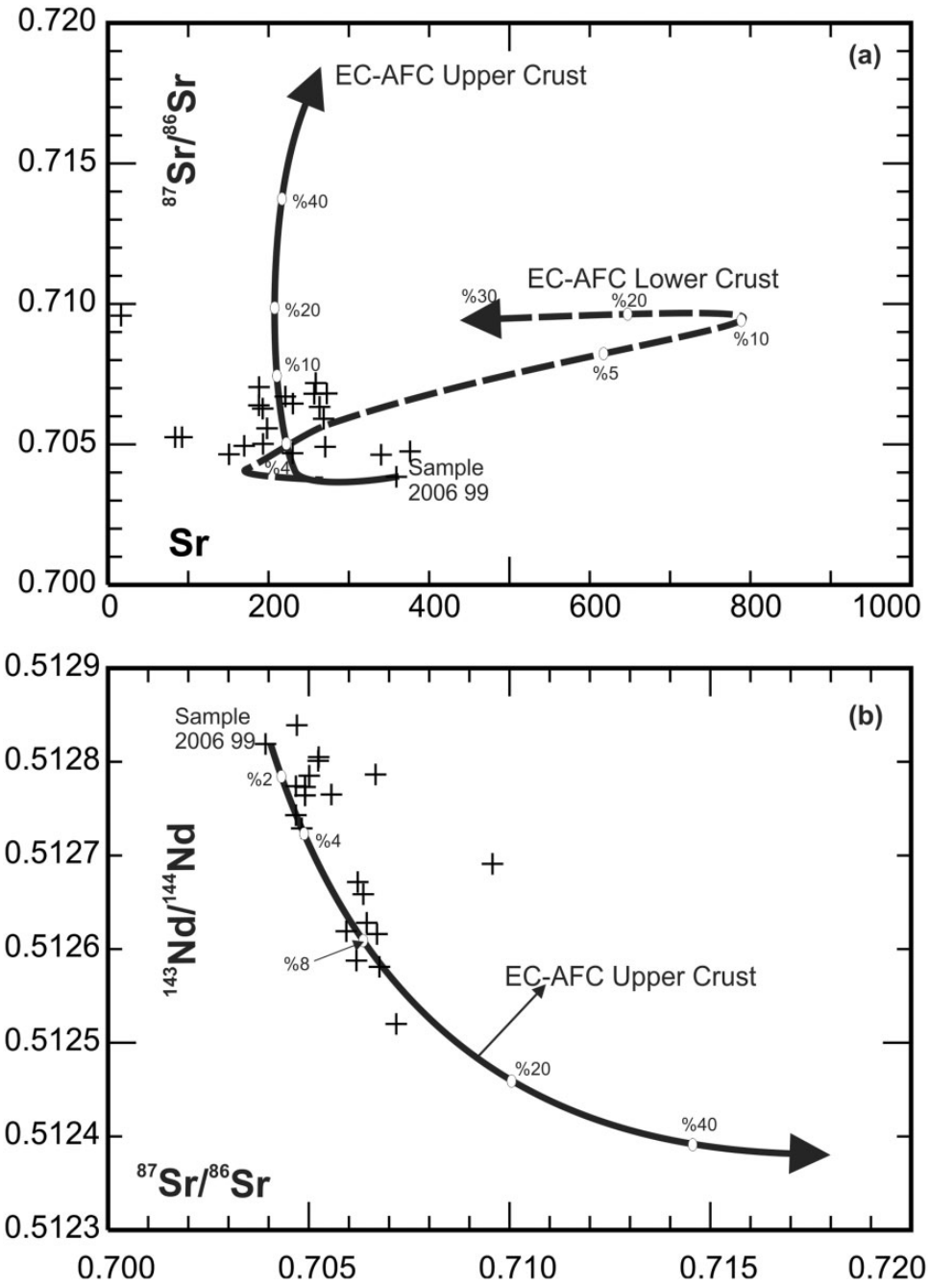


Fig. 11. $^{87}Sr/^{86}Sr$ vs Sr (ppm) (a) and $^{143}Nd/^{144}Nd$ vs $^{87}Sr/^{86}Sr$ (b) with EC-AFC curves calculated using the model of Bohrson & Spera (2001). Small ellipses on the curves indicate the percentage of assimilated contaminant. Bulk distribution coefficients are calculated using the modal mineralogy of sample 2006 99 ($Plagioclase_{0·5} + Clinopyroxene_{0·3} + Olivine_{0·18} + Ilmenite_{0·02}$). Partition coefficients of elements used for EC-AFC modelling are from the Geochemical Earth Reference Model home page (http://www.earthref.org).

proposed to have formed from subducted terrigenous sediments (Weaver, 1991), recycling of delaminated subcontinental lithosphere into the mantle (e.g. Hawkesworth *et al.*, 1986, 1988, 1990) and the presence of a pyroxenitic component derived from previous subduction-related magmatic rocks within the lithosphere (Timm *et al.*, 2009).

Tectono-magmatic history and role of lithospheric mantle

The nature and the source of the magmatism in eastern Anatolia is still a matter of debate. There are several hypotheses about the origin of the magmatism and lithospheric structure beneath eastern Anatolia. The two main

Downloaded from https://academic.oup.com/petrology/article-abstract/55/1/37/1524170 by Yuzuncu Yil University user on 23 April 2020

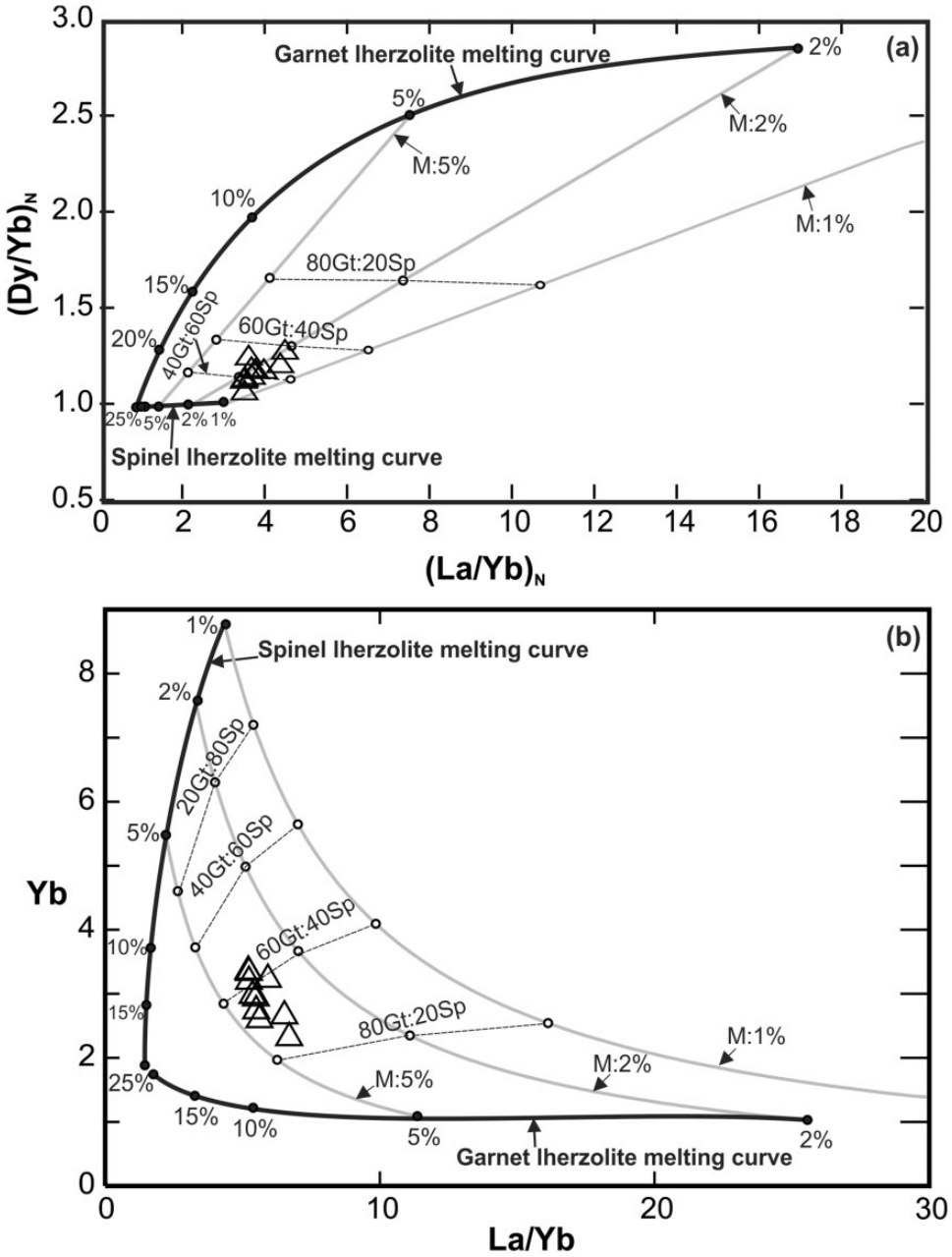


Fig. 12. $(Dy/Yb)_N$ vs $(La/Yb)_N$ (a), Yb vs La/Yb (b) variations in Süphan volcanic rocks compared with calculated partial melting curves assuming non-modal batch melting of garnet (Gt) and spinel (Sp) lherzolite sources (garnet lherzolite: 0·598 ol, 0·211 opx, 0·076 cpx, 0·115 grt, melting proportions: 0·05 ol, 0·2 opx, 0·3 cpx, 0·45 grt; spinel lherzolite: 0·578 ol, 0·27 opx, 0·119 cpx, 0·033 sp, melting proportions: 0·1 ol, 0·27 opx, 0·5 cpx, 0·13 sp; Thirlwall *et al.*, 1994; Shaw *et al.*, 2003; Peters *et al.*, 2008). The concentrations of La, Yb and Dy have been corrected to 7 wt % MgO to correct for the majority of AFC effects. The slopes, intercepts and r^2 values for all regressions against MgO are given in Table 5. The composition of the primitive mantle and distribution coefficients are from McKenzie & O'Nions (1991). M:1%, M:2% and M:5% represent mixing lines between 1%, 2% and 5% melts of garnet and spinel peridotite. Dashed lines represent the relative proportions of melts from garnet and spinel peridotite in the parental magmas.

models proposed are partial lithospheric delamination (Pearce *et al.*, 1990) and slab break-off (Keskin, 2003; Şengör *et al.*, 2003). Pearce *et al.* (1990) proposed delamination of the lower lithosphere as the main reason for the widespread volcanism in eastern Anatolia. Following recent seismic studies (since 2003) concerned with the lithospheric structure in eastern Anatolia (ETSE, Eastern Turkey Seismic Experiment), the geochemical characteristics of the eastern Anatolian volcanic rocks have been evaluated in the light of the new geophysical data. Keskin

Downloaded from https://academic.oup.com/petrology/article-abstract/55/1/37/1524170 by Yuzuncu Yil University user on 23 April 2020

Table 5: Regression details for fractionation correction of Süphan trace element data to 7 wt % MgO

Element	Slope	Intercept	r^2
ppm			
Ba	−58·50	550·13	0·89
Th	−1·85	15·24	0·89
Sm	−0·78	10·38	0·76
Dy	−0·67	10·04	0·76
Yb	−0·32	5·16	0·57
La	−3·88	43·77	0·93

(2003) claimed that volcanic activity in eastern Anatolia began earlier in the north (11–13 Ma) than in the south, migrating towards the south with time. This migration was accompanied by changes in magma chemistry in a north–south direction. The volcanic products erupted in the north around the Erzurum–Kars plateau are calc-alkaline in character with a distinct subduction signature. Volcanic rocks in the south around the Mus–Nemrut–Tendürek volcanoes are alkaline with an intraplate signature (Pearce *et al.*, 1990). The volcanic rocks of the Bingöl and Süphan volcanoes (Fig. 1a) display transitional chemical characteristics. However, the data accumulated so far for the eastern Anatolian volcanic rocks support neither a monotonic age progression nor any systematic change in geochemical characteristics with time from north to south (e.g. 15 Ma Aladağ andesites (Lebedev *et al.*, 2010) and 11·9–12·6 Ma Sarıçimen quartz monzodiorites (Çolakoğlu & Arehart, 2010) are both situated in the southern part of eastern Anatolia). The non-uniform distribution of ages and geochemical characteristics of the volcanic rocks, along with the recent results of geophysical studies (e.g. Sandvol *et al.*, 2003*a*, 2003*b*; Zor *et al.*, 2003; Angus *et al.*, 2006; Gök *et al.*, 2007; Özacar *et al.*, 2008) in eastern Anatolia, cast doubt on validity of only a lithospheric mantle source (e.g. Pearce *et al.*, 1990; Yilmaz *et al.*, 1998; Kheirkhah *et al.*, 2009) or only an asthenospheric mantle source, with or without a subduction component (Keskin, 2003, 2007; Şengör *et al.*, 2008), in the generation of the widespread volcanism in the region.

To evaluate the relative roles of lithospheric and asthenospheric mantle sources, as well as the melting degree and melting depth, Süphan volcanic rocks are compared here with data for other volcanic rocks of the region from previous studies (Gülen, 1984; Pearce *et al.*, 1990; Arslan, 1994; Buket & Temel, 1998; Özdemir *et al.*, 2006; Kheirkhah *et al.*, 2009; Lustrino *et al.*, 2010, Supplementary Data Table 3). For this purpose, to avoid the effects of fractional crystallization, only rocks with <53 wt % SiO_2 and >4·5 wt % MgO were chosen (Supplementary Data Table 3). Data that are used for interpretations are grouped into Miocene–Pliocene (Erzurum–Kars, Muş, Meydan) and Quaternary lavas (Ağrı, Nemrut, Süphan, Tendürek). Karacadağ volcanic rocks (on the Arabian Foreland) that display within-plate characteristics are also shown for comparison.

Concentrations of REE can be used to provide evidence for the presence of garnet in the source of the parental magmas to the volcanic rocks. Garnet strongly retains the HREE, and therefore magmas derived from a garnet-bearing source should have high LREE/HREE (Blundy *et al.*, 1998). La/Yb ratios are in the range of 12·67–16·09 for Meydan, 5·70–14·04 for Erzurum–Kars, 6·59–8·93 for Muş, 4·49–8·19 for Tendürek, 4·35–7·97 for Ağrı, and 4·81–7·73 for Nemrut; the ratio is 5·14 for Süphan. It is apparent that the La/Yb ratio decreases from the Miocene–Pliocene (Meydan, Erzurum–Kars, Muş) to the Quaternary (Tendürek, Ağrı, Nemrut, Süphan) volcanic fields. The MREE/HREE ratio Dy/Yb may also indicate the presence of garnet in the mantle source region. All of the eastern Anatolian volcanic rocks have $(Dy/Yb)_N > 1·06$ further supporting the presence of garnet in the mantle source. Further contraints can be made using a Sm/Yb vs La/Sm diagram (Fig. 14). The Miocene–Pliocene lavas plot along mixing lines between 0·7 and 3% melts of garnet- and spinel-facies peridotite. The contribution of the garnet- and spinel-facies peridotite in the genesis of these magmas seems to correspond to a garnet/spinel peridotite ratio between ~75/25 and 60/40. However, the garnet/spinel peridotite ratio for the two volcanic samples from Erzurum–Kars is 40/60. Quaternary lavas from eastern Anatolia (Ağrı, Nemrut, Süphan, Tendürek) plot in a different position in the diagram. It is apparent from Fig. 14 that the garnet contribution in the petrogenesis of the parental magmas decreases from Miocene–Pliocene to Quaternary times, accompanied by an increase in melting degree (up to 5%). On the other hand, mafic Karacadağ volcanic rocks on the Arabian Foreland are consistent with various degrees of melting between 1 and 2% and have a garnet peridotite contribution of more than 80% in their petrogenesis.

Geophysical studies have indicated that the eastern Anatolian crust has an average thickness of ~45 km (e.g. Çakır *et al.*, 2000; Zor *et al.*, 2003) and varies from about 38 km to 50 km from south (Arabian foreland) to north (Pontides mountain range). The mantle part of the lithosphere is absent (e.g. Al-Lazki *et al.*, 2003; Sandvol *et al.*, 2003*a*; Gök *et al.*, 2007) or thin (e.g. Angus *et al.*, 2006; Özacar *et al.*, 2008) beneath eastern Anatolia. The studies of Angus *et al.* (2006) and Özacar *et al.* (2008) suggested an average thickness of 75 km for the eastern Anatolian lithosphere. This thickness is less than the normal thickness of continental lithosphere, although it still implies the

Downloaded from https://academic.oup.com/petrology/article-abstract/55/1/37/1524170 by Yuzuncu Yil University user on 23 April 2020

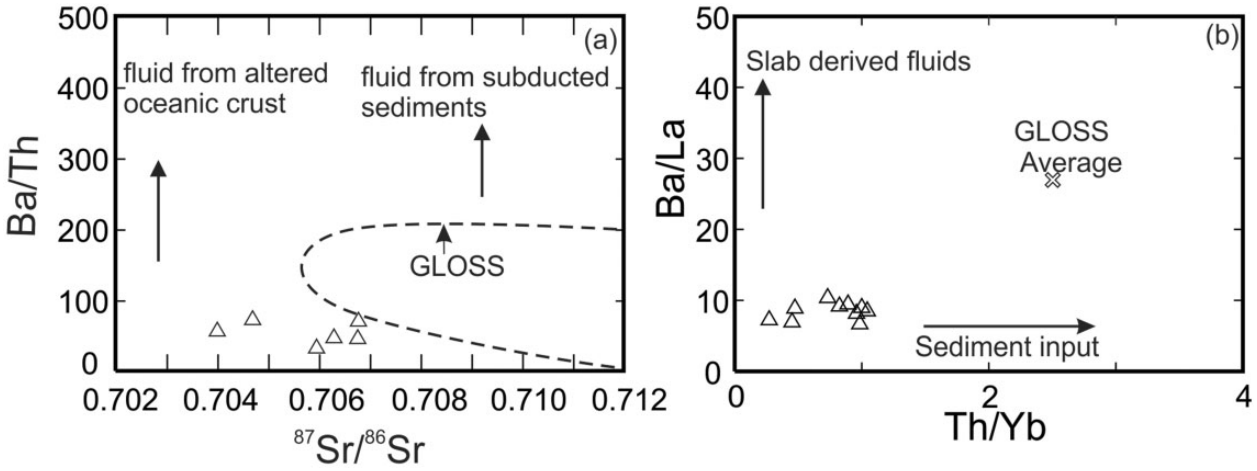


Fig. 13. (a) Ba/Th vs $^{87}Sr/^{86}Sr$, (b) Ba/La vs Th/Yb, for Süphan volcanic rocks. Symbols are the same as in Fig. 14. GLOSS and GLOSS average are from Plank & Langmuir (1998). The concentrations of Ba, La, Th and Yb have been corrected to 7 wt % MgO to correct for the majority of AFC effects. The slopes, intercepts and r^2 values for all regressions against MgO are given in Table 5.

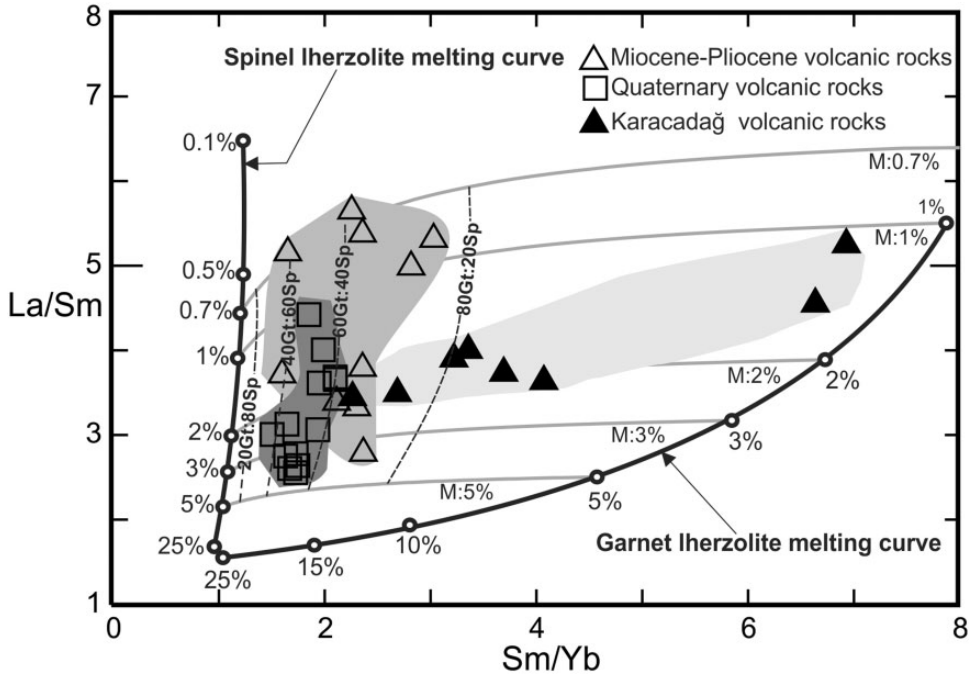


Fig. 14. Calculated partial melting curves assuming non-modal batch melting of garnet (Gt) and spinel (Sp) lherzolite sources compared with eastern Anatolian volcanic rocks in a Sm/Yb vs La/Sm diagram (garnet lherzolite: 0·598 ol, 0·211 opx, 0·076 cpx, 0·115 grt; melting proportions: 0·05 ol, 0·2 opx, 0·3 cpx, 0·45 grt; spinel lherzolite: 0·578 ol, 0·27 opx, 0·119 cpx, 0·033 sp; melting proportions: 0·1 ol, 0·27 opx, 0·5 cpx, 0·13 sp; Thirlwall *et al.*, 1994; Shaw *et al.*, 2003; Peters *et al.*, 2008). The composition of the primitive mantle and distribution coefficients are from McKenzie & O'Nions (1991). M:0·7%, M:1%, M:2%, M:3%, and M:5% represents mixing lines between 0·7%, 1%, 2%, 3% and 5% melts of garnet and spinel peridotite. Data sources for eastern Anatolian volcanics are given in Supplementary Material 3. Dashed lines indicate the relative proportions of melts derived from garnet and spinel peridotite mantle sources contributing to the parental magmas.

presence of mantle lithosphere beneath the crust of eastern Anatolia. Thin lithospheric mantle beneath the region can be re-formed by melting and cooling of the asthenosphere (Keskin, 2007) or may represent a remnant of older lithospheric mantle prior to asthenospheric upwelling. Angus *et al.* (2006) proposed that the 15–22 km thick mantle lithosphere could have been re-formed by cooling of the asthenosphere for times of 7 and 15 Ma respectively. However, Şengör *et al.* (2008) argued against the re-forming of the mantle lithosphere beneath the region on the

Downloaded from https://academic.oup.com/petrology/article-abstract/55/1/37/1524170 by Yuzuncu Yil University user on 23 April 2020

basis of their temporal and thermal lithospheric evolution model.

With the spinel to garnet transition at a depth of ~80 km (Takahashi & Kushiro, 1983), it is likely that spinel peridotite facies (<80 km) comprises most of the lower lithosphere beneath eastern Anatolia. Garnet peridotite facies (>80 km) is primarily part of the asthenosphere beneath the region. Melting trajectories based on the available data suggest that the parental eastern Anatolian magmas are the result of various degrees of mixing between asthenospheric and lithospheric melts. To a crude approximation, melting degree and the contribution of the spinel peridotite facies source (lithospheric mantle contribution) increases from Miocene–Pliocene to Quaternary times. Most models for post-collisional magmatism predict that the magmatism should change from lithospheric to intra-plate asthenospheric melts with time (e.g. Pearce *et al.*, 1990; Turner *et al.*, 1992, 1996; Maheo *et al.*, 2002). However, the reverse progression is observed in eastern Anatolia. The lithospheric contribution appears to be progressively increasing from Miocene–Pliocene to Quaternary times. Similar transitions have been reported in the Betic–Alboran domain in SE Spain (Turner *et al.*, 1999) and northern Taiwan (Wang *et al.*, 2004). Significant differences in the amount of thickened crust in different collision zones, the rheology of the two plates in collision, the extent of the collision and the velocity of plate convergence, are all important controls on the geochemical characteristics and time interval between the onset of collision and the generation of post-collisional magmatism (Turner *et al.*, 1999; Wang *et al.*, 2004). Both slab break-off and partial loss of the lower lithosphere can be responsible for asthenospheric upwelling and widespread volcanism in the region.

CONCLUSIONS

The Süphan stratovolcano, representing one of the major eruption centers of the post-collisional volcanism in eastern Anatolia, consists of lava flows, domes and pyroclastic rocks, ranging in composition from basalt to rhyolite. Geochemical data reveal a transitional mildly alkaline to calc-alkaline character for the eruptive products. New ^{40}Ar–^{39}Ar age data for samples from different levels of the stratigraphic succession, combined with previous K/Ar ages, yield a range of 0·76–0·06 Ma.

Geochemical modeling of major element compositions suggests that relatively mafic ($SiO_2 \leq 55$ wt %) and SiO_2-rich ($SiO_2 > \sim 65$ wt %) members of the Süphan volcanic suite evolved at moderately hydrated ($H_2O = 1$ wt %) and oxidizing QFM (quartz–fayalite–magnetite) conditions at 2–4 kbar pressure. On the other hand, most of the lavas with SiO_2 contents between ~57 and ~65 wt % are products of isobaric–isenthalpic mixing of 70% basaltic trachyandesitic magma (at 1100°C) and 30% rhyolitic magma (at 900°C) at a crustal pressure of 0·5 kbar.

EC-AFC modeling of trace element and isotope compositions indicates that this crustal differentiation was accompanied by assimilation of upper crustal rocks that contaminated the Süphan magmas by ~2–10%.

LILE enrichment and the presence of negative HFSE (Nb and Ta in particular) anomalies in primitive mantle-normalized element patterns suggest similarities with magmas generated in subduction-related tectonic settings. Ba/Th, Pb/Ce, Ba/La, Th/Ce and $^{206}Pb/^{204}Pb$, $^{207}Pb/^{204}Pb$ and $^{208}Pb/^{204}Pb$ ratios are consistent with the mantle source of the Süphan magmas being modified by subducted sediments.

Based on LREE/HREE, MREE/HREE ratios and partial melting models, we suggest that the eastern Anatolian parental magmas are products of variable degrees of mixing of magmas derived from asthenospheric and lithospheric mantle sources. As opposed to most models for post-collisional magmatism that predict a change from lithospheric to intra-plate asthenospheric melts with time, the melting degree and contribution of the lithospheric mantle appears to have increased from Miocene–Pliocene to Quaternary times in eastern Anatolia. This may be ascribed to the heat driven by asthenospheric upwelling subsequent to the partial loss of the lower lithosphere beneath the region via mechanical delamination or slab break-off.

ACKNOWLEDGEMENTS

We thank A. Ü. Tolluoğlu, V. Toprak and M. Lütfi Süzen for discussions on the geology of the Süphan stratovolcano. We also thank Terry Spell from the University of Nevada, Las Vegas for critical reviews on ^{40}Ar–^{39}Ar radiometric age data. We are grateful to Marjorie Wilson, John Gamble, Julian Pearce and two anonymous reviewers for extremely helpful and constructive comments.

FUNDING

This work has been funded by both Middle East Technical University Scientific Research Project Foundation (ÖYP Project) and TÜBİTAK, the Scientific and Technical Research Council of Turkey (Project No. YDABAG 104Y372).

SUPPLEMENTARY DATA

Supplementary data for this paper are available at *Journal of Petrology* online.

REFERENCES

Agard, P., Omrani, J., Jolivet, L. & Mouthereau, F. (2005). Convergence history across Zagros (Iran): Constraints from

Downloaded from https://academic.oup.com/petrology/article-abstract/55/1/37/1524170 by Yuzuncu Yil University user on 23 April 2020

collisional and earlier deformation. *International Journal of Earth Sciences* **94**, 401–419.

Alavi, M. (1994). Tectonics of the Zagros orogenic belt of Iran—New data and interpretations. *Tectonophysics* **229**, 211–238.

Al-Lazki, A., Seber, D., Sandvol, E., Turkelli, N., Mohamad, R. & Barazangi, M. (2003). Tomographic Pn velocity and anisotropy structure beneath the Anatolian plateau (eastern Turkey) and the surrounding regions. *Geophysical Research Letters* **30**, doi:10.1029/2003GL017391.

Allen, M. & Armstrong, H. A. (2008). Arabia–Eurasia collision and the forcing of mid-Cenozoic global cooling. *Palaeogeography, Palaeoclimatology, Palaeoecology* **265**, 52–58.

Angus, D. A., Wilson, D. C., Sandvol, E. & Ni, J. F. (2006). Lithospheric structure of the Arabian and Eurasian collision zone in Eastern Turkey from S-wave receiver functions. *Geophysical Journal International* **166**, 1335–1346.

Arslan, M. (1994). Mineralogy, geochemistry, petrology and petrogenesis of the Meydan–Zilan (Erciş–Van, Turkey) area volcanic rocks. PhD thesis, University of Glasgow, 559 pp.

Berberian, M. & King, G. (1981). Toward a paleogeography and tectonic evolution of Iran. *Canadian Journal of Earth Sciences* **18**, 210–265.

Blundy, J. D., Robinson, J. A. C. & Wood, B. J. (1998). Heavy REE are compatible in clinopyroxene on the spinel lherzolite solidus. *Earth and Planetary Science Letters* **160**, 493–504.

Bohrson, W. A. & Spera, F. J. (2001). Energy-constrained open-system magmatic processes II: application of energy-constrained assimilation–fractional crystallisation (EC-AFC) model to magmatic systems. *Journal of Petrology* **42**, 1019–1041.

Bryan, W. B., Finger, I. & Chayes, F. (1969). Estimating proportions in petrographic mixing equations by least-square approximation. *Science* **163**, 926–927.

Buket, E. & Temel, A. (1998). Major-element, trace-element, and Sr–Nd isotopic geochemistry and genesis of Varto Mus, volcanic rocks, Eastern Turkey. *Journal of Volcanology and Geothermal Research* **85**, 405–422.

Çakır, Ö., Erduran, M., Çınar, H. & Yılmaztürk, A. (2000). Forward modeling receiver functions for crustal structure beneath station TBZ (Trabzon,Turkey). *Geophysical Journal International* **140**, 341–356.

Class, C., Miller, D. M., Goldstein, S. L. & Langmuir, C. H. (2000). Distinguishing melt and fluid subduction components in Umnak volcanics: Aleutian arc. *Geochemistry, Geophysics, Geosystems* **1**, 1999GC000010.

Çolakoğlu, A. L. & Arehart, G. B. (2010). The petrogenesis of Sarıçimen (Çaldıran–Van) quartz monzodiorite: Implication for initiation of magmatism (Late Medial Miocene) in the east Anatolian collision zone, Turkey. *Lithos* **119**, 607–620.

De Paolo, D. J. (1981). Trace element and isotopic effects of combined wall rock assimilation and fractional crystallization. *Earth and Planetary Science Letters* **53**, 189–202.

Dewey, J. F., Hempton, M. R., Kidd, W. S. F., Şaroğlu, F. & Şengör, A. M. C. (1986). Shortening of continental lithosphere: the neotectonics of Eastern Anatolia—a young collision zone. In: Coward, M. P. & Ries, A. C. (eds) *Collision Tectonics. Geological Society, London, Special Publications* **19**, 3–36.

Elburg, M. A., Bergen, M. V., Hoogewerff, J., Foden, J., Vroon, P., Zulkarnain, I. & Nasution, A. (2002). Geochemical trends across an arc–continent collision zone: magma sources and slab–wedge transfer processes below the Pantar Strait volcanoes, Indonesia. *Geochimica et Cosmochimica Acta* **66**, 2771–2789.

Elliott, T., Planck, T., Zindler, A., White, W. & Bourdon, B. (1997). Element transport from slab to volcanic front at the Mariana arc. *Journal of Geophysical Research* **102**, 14991–15019.

Ercan, T., Fujitani, T., Matsuda, J., Notsu, K., Tokel, S. & Tadahide, U. İ. (1990). Doğu ve Güneydoğu Anadolu Neojen-Kuvaterner volkanitlerine ilişkin yeni jeokimyasal, radyometrik ve izotopik verilerin yorumu. *MTA dergisi* **110**, 143–164.

Ghiorso, M. S. & Sack, R. O. (1995). Chemical transfer in magmatic processes IV. A revised and internally consistent thermodynamic model for the interpolation and extrapolation of liquid–solid equilibria in magmatic systems at elevated temperatures and pressures. *Contributions to Mineralogy and Petrology* **119**, 197–212.

Gök, R., Pasyanos, M. E. & Zor, E. (2007). Lithospheric structure of the continent–continent collision zone: eastern Turkey. *Geophysical Journal International* **169**, 1079–1088.

Gülen, L. (1984). Sr, Nd, Pd isotope and trace elements geochemistry of calc-alkaline and alkaline volcanics, eastern Turkey. PhD thesis, Massachussets Institute of Technology, Cambridge, MA, 229 pp.

Guo, Z., Hertogen, J., Liu, J., Pasteels, P., Boven, A., Punzalan, L., He, H., Luo, X. & Zhang, W. (2005). Potassic magmatism in western Sichun and Yunnan provinces, SE Tibet, China: petrological and geochemical constraints on petrogenesis. *Journal of Petrology* **46**, 33–78.

Guo, Z., Wilson, M., Liu, J. & Mao, Q. (2006). Post-collisional, potassic and ultrapotassic magmatism of the northern Tibetan Plateau: constraints on characteristics of the mantle source, geodynamic setting and uplift mechanisms. *Journal of Petrology* **47**, 1177–1220.

Hall, R. (1976). Ophiolite emplacement and the evolution of the Taurus suture zone, southeastern Turkey. *Geological Society of America Bulletin* **87**, 1078–1088.

Hart, S. R. (1984). A large-scale isotope anomaly in the Southern Hemisphere mantle. *Nature* **309**, 753–57.

Hawkesworth, C. J., Taylor, P. N. & Palacz, Z. (1986). Evidence from the Parana of South Brazil for a continental contribution to Dupal basalts. *Nature* **322**, 356–359.

Hawkesworth, C. J., Mantovani, M. S. M. & Peate, D. W. (1988). Lithosphere remobilisation during Parana CFB magmatism. In: Cox, K. G. & Menzies, M. A. (eds) *Oceanic and Continental Lithosphere: Similarities and Differences. Journal of Petrology, Special Volume*, pp. 205–223.

Hawkesworth, C. J., Kempton, P. D., Rogers, N. W., Ellam, R. M. & Von Calsteren, P. W. (1990). Continental mantle lithosphere and shallow level enrichment processes in the Earth's mantle. *Earth and Planetary Science Letters* **96**, 256–268.

Hawkesworth, C. J., Gallagher, K., Hergt, J. M. & McDermott, F. (1993). Mantle and slab contributions in arc magmas. *Annual Review of Earth and Planetary Sciences* **21**, 175–204.

Hawkesworth, C. J., Turner, S. P., McDermott, F., Peate, D. W. & van Calsteren, P. (1997). U–Th isotopes in arc magmas: implications for element transfer from the subducted crust. *Science* **276**, 551–555.

Innocenti, F., Mazzuoli, R., Pasquare, G., Redicat di Brozolo, F. & Villari, L. (1976). Evolution of the volcanism in the area of interaction between the Arabian, Anatolian and Iranian plates (Lake Van, Eastern Turkey). *Journal of Volcanology and Geothermal Research* **1**, 103–112.

Innocenti, F., Manetti, P., Mazzuoli, R., Pasquaré, G. & Villari, L. (1982*a*). Anatolia and north-western Iran. In: Thorpe, R. S. (ed.) *Andesites*. John Wiley, pp. 327–349.

Innocenti, F., Mazzuoli, R., Pasquaré, G., Radicati di Brozolo, F. & Villari, L. (1982*b*). Tertiary and Quaternary volcanism of the Erzurum–Kars area (Eastern Turkey): Geochronological data and geodynamic evolution. *Journal of Volcanology and Geothermal Research* **13**, 223–240.

Jolivet, L. & Faccenna, C. (2000). Mediterranean extension and the Africa–Eurasia collision. *Tectonics* **19**, 1095–1106.

Downloaded from https://academic.oup.com/petrology/article-abstract/55/1/37/1524170 by Yuzuncu Yil University user on 23 April 2020

Justet, L. & Spell, T. L. (2001). Effusive eruptions from a large silicic magma chamber: The Bearhead Rhyolite, Jemez volcanic field, N.M. *Journal of Volcanology and Geothermal Research* **107**, 241–264.

Karaoğlu, Ö., Özdemir, Y., Tolluoğlu, A. Ü., Karabıyıkoğlu, M., Köse, O. & Froger, J. L. (2005). Stratigraphy of the volcanic products around Nemrut Caldera: Implications for reconstruction of the caldera formation. *Turkish Journal of Earth Sciences* **14**, 123–143.

Keskin, M. (2003). Magma generation by slab steepening and breakoff beneath a subduction–accretion complex: An alternative model for collision-related volcanism in Eastern Anatolia, Turkey. *Geophysical Research Letters* **30**, 1–4, doi:10.1029/2003GL018019.

Keskin, M. (2007). Eastern Anatolia: a hot spot in a collision zone without a mantle plume. In: Foulger, G. R. & Jurdy, D. (eds) *Plates, Plumes, and Planetary Processes. Geological Society of America, Special Papers* **430**, 693–722.

Keskin, M., Pearce, J. A. & Mitchell, J. G. (1998). Volcano-stratigraphy and geochemistry of collision-related volcanism on the Erzurum–Kars Plateau, North Eastern Turkey. *Journal of Volcanology and Geothermal Research* **85**, 355–404.

Kheirkhah, M., Allen, M. B. & Emami, M. (2009). Quaternary syn-collision magmatism from the Iran/Turkey borderlands. *Journal of Volcanology and Geothermal Research* **182**, 1–12.

Klein, E. & Langmuir, C. (1987). Global correlations of ocean ridge basalt chemistry with axial depth and crustal thickness. *Journal of Geophysical Research* **92**, 8089–8115.

Koçyiğit, A., Yılmaz, A., Adamina, S. & Kuloshvili, S. (2001). Neotectonics of East Anatolian Plateau (Turkey) and Lesser Caucasus: implication for transition from thrusting to strike-slip faulting. *Geodinamica Acta* **14**, 177–195.

Langmuir, C., Vocke, R., Hanson, G. & Hart, S. (1978). A general mixing equation with applications to Icelandic basalts. *Earth and Planetary Science Letters* **37**, 380–392.

Lebedev, V. A., Sharkov, E. V., Keskin, M. & Oyan, V. (2010). Erratum: Geochronology of Late Cenozoic volcanism in the area of Lake Van, Turkey: an example of developmental dynamics for magmatic processes. *Doklady Earth Sciences* **433(2)**, 1031–1037.

Lustrino, M., Keskin, M., Mattioli, M., Lebedev, V., Chugaev, A., Sharkov, E. & Kavak, O. (2010). Early activity of the largest Cenozoic shield volcano in the circum-Mediterranean area: Mt. Karacadağ, SE Turkey. *European Journal of Mineralogy* **22**, 343–362.

Maheo, G., Guillot, S., Blichert-Toft, J., Rolland, Y. & Pecher, A. (2002). A slab breakoff model for the Neogene thermal evolution of South Karakorum and South Tibet. *Earth and Planetary Science Letters* **195**, 45–58.

McKenzie, D. P. & O'Nions, R. K. (1991). Partial melt distributions from inversion of rare earth element concentrations. *Journal of Petrology* **32**, 1021–1091.

Mutlu, H., Güleç, N., Hilton, D. R., Aydın, H. & Halldórsson, S. A. (2012). Spatial variations in gas and stable isotope compositions of thermal fluids around Lake Van: Implications for crust–mantle dynamics in eastern Turkey. *Chemical Geology* **300–301**, 165–176.

Nakamura, N. (1974). Determination of REE, Ba, Mg, Na and K in carbonaceous and ordinary chondrites. *Geochimica et Cosmochimica Acta* **38**, 757–775.

Notsu, K., Fujitoni, T., Ui, T., Matsuda, J. & Ercan, T. (1995). Geochemical features of collision related volcanic rocks in central and Eastern Anatolia, Turkey. *Journal of Volcanology and Geothermal Research* **64**, 171–192.

Ogata, A., Nakamura, K., Nagao, K. & Akimoto, S. (1989). K-Ar age of young volcanic rocks of Turkey. *Annual meeting of the Geochemical Society of Japan*, ICO 3.

Okay, A. I., Zattin, M. & Cavazza, W. (2010). Apatite fission-track data for the Miocene Arabia–Eurasia collision. *Geology* **38**, 35–38.

Oyan, V. (2011). Etrüsk Volkanı ve Çevresinin (Van Gölü Kuzeyi) Volkanostratigrafisi Petrolojisi ve Magmatik Evrimi, Doctoral thesis, Yuzuncu Yil University, Van, 375 pp.

Özacar, A. A., Gilbert, H. & Zandt, G. (2008). Upper mantle discontinuity structure beneath East Anatolian Plateau (Turkey) from receiver functions. *Earth and Planetary Science Letters* **269**, 426–434.

Özdemir, Y., Karoğlu, Ö., Tolluoğlu, A. Ü. & Güleç, N. (2006). Volcanostratigraphy and petrogenesis of the Nemrut stratovolcano (East Anatolian High Plateau): The most recent post-collisional volcanism in Turkey. *Chemical Geology* **226**, 189–211.

Özdemir, Y., Karaoğlu, Ö., Tolluoğlu, A. Ü. & Güleç, N. (2007). Reply to discussion by Evren Çubukçu, Erkan Aydar and Alain Gourgaud of 'Volcanostratigraphy and petrogenesis of the Nemrut stratovolcano (East Anatolian High Plateau): The most recent post-collisional volcanism in Turkey' by Y. Özdemir, Ö. Karaoğlu, A. Ü. Tolluoğlu and N. Güleç. *Chemical Geology* **245**, 130–134.

Özdemir, Y., Blundy, J. D. & Güleç, N. (2011). The importance of fractional crystallization and magma mixing in controlling chemical differentiation at Süphan Stratovolcano, Eastern Anatolia, Turkey. *Contributions to Mineralogy and Petrology* **162**, 573–597.

Pearce, J. A., Bender, J. F., De Long, S. E., Kidd, W. S. F., Low, P. J., Güner, Y., Şaroğlu, F., Yılmaz, Y., Moorbath, S. & Mitchell, J. G. (1990). Genesis of collision volcanism in Eastern Anatolia, Turkey. *Journal of Volcanology and Geothermal Research* **44**, 189–229.

Peters, T. J., Menzies, M., Thirlwall, M. & Kyle, P. (2008). Zuni–Bandera volcanism, Rio Grande, USA—melt formation in garnet- and spinel-facies mantle straddling the asthenosphere–lithosphere boundary. *Lithos* **102**, 295–315.

Plank, T. & Langmuir, C. H. (1998). The chemical composition of subducting sediment and its consequences for the crust and mantle. *Chemical Geology* **145**, 325–394.

Robertson, A. H. F., Parlak, O., Rızaoğlu, T., Ünlügenç, Ü., İnan, N., Taslı, K. & Ustaömer, T. (2007). Tectonic evolution of the South Tethyan ocean: Evidence from the Eastern Taurus Mountains (Elazığ region, SE Turkey). In: Ries, A. C., Butler, R. W. H. & Graham, R. H. (eds) *Deformation of Continental Crust. Geological Society, London, Special Publications* **272**, 231–270.

Ryan, J. G., Morris, J., Tera, F., Leeman, W. P. & Tsvetskov, A. (1995). Cross-arc geochemical variations in the Kurile arc as a function of slab depth. *Science* **270**, 625–627.

Sandvol, E., Türkelli, N. & Barazangi, M. (2003*a*). The eastern Turkey seismic experiment: the study of a young continent–continent collision. *Geophysical Research Letters* **30(24)**, doi:10.1029/2003GL018912.

Sandvol, E., Türkelli, N., Zor, E., Gok, R., Bekler, T., Gürbüz, C., Seber, D. & Barazangi, M. (2003*b*). Shear wave splitting in a young continent–continent collision: an example from Eastern Turkey. *Geophysical Research Letters* **30(24)**, 8041, doi:10.1029/2003GL017390.

Şen, P. A., Temel, A. & Gourgaud, A. (2004). Petrogenetic modeling of Quaternary post- collisional volcanism: a case study of central and eastern Anatolia. *Geological Magazine* **141**, 81–98.

Şengör, A. M. C. (1990). A new model for the late Palaeozoic–Mesozoic tectonic evolution of Iran and implications for Oman. In: Robertson, A. H. F., Searle, M. P. & Ries, A. C. (eds) *The Geology and Tectonics of the Oman Region. Geological Society, London, Special Publications* **49**, 797–831.

Şengör, A. M. C. & Kidd, W. S. F. (1979). Post-collisional tectonics of the Turkish–Iranian plateau and a comparison with Tibet. *Tectonophysics* **55**, 361–376.

Şengör, A. M. C., Görür, N. & Şaroğlu, F. (1985). Strike-slip faulting and related basin formation in zones of tectonic escape: Turkey as a case study. In: Biddle, K. D. & Christie-Blick, N. (eds) *Strike-Slip*

Downloaded from https://academic.oup.com/petrology/article-abstract/55/1/37/1524170 by Yuzuncu Yil University user on 23 April 2020

Deformation, Basin Formation and Sedimentation. Society of Economic Paleontologists and Mineralogists, Special Publications **17**, 227–264.

Şengör, A. M. C., Özeren, S., Genç, T. & Zor, E. (2003). East Anatolian high plateau as a mantle supported, north–south shortened domal structure. *Geophysical Research Letters* **30**, doi:10.1029/2003GL017858.

Şengör, A. M. C., Özeren, S., Keskin, M., Sakınç, M., Özbakir, A. D. & Kayan, I. (2008). Eastern Turkish high plateau as a small Turkic-type orogen: Implications for post-collisional crust-forming processes in Turkic-type orogens. *Earth-Science Reviews* **90**, 1–48.

Shaw, D. M. (1970). Trace element fractionation during anatexis. *Geochimica et Cosmochimica Acta* **34**, 237–243.

Shaw, J. E., Baker, J. A., Menzies, M. A., Thirlwall, M. F. & Ibrahim, K. M. (2003). Petrogenesis of the largest intraplate volcanic field on the Arabian Plate (Jordan): a mixed lithosphere–asthenosphere source activated by lithospheric extension. *Journal of Petrology* **44**, 1657–1679.

Sheppard, S. & Taylor, W. R. (1992). Barium and LREE-rich, olivine–mica-lamprophyres with affinities to lamproites, Mt. Bundey, Northern Territory, Australia. *Lithos* **28**, 303–325.

Spell, T. L. & McDougall, I. (2003). Characterization and calibration of $^{40}Ar/^{39}Ar$ dating standards. *Chemical Geology* **198(3–4)**, 189–211.

Spera, F. J. & Bohrson, W. A. (2001). Energy-constrained open-system magmatic processes I: general model and energy-constrained assimilation–fractional crystallisation (EC-AFC) formulation. *Journal of Petrology* **42**, 999–1018.

Staudacher, Th., Jessberger, E. K., Dorflinger, D. & Kiko, J. (1978). A refined ultra-high vacuum furnace for rare gas analysis. *Journal of Physics E: Scientific Instruments* **11**, 781–784.

Sun, S.-S. & McDonough, W. F. (1989). Chemical and isotopic systematics of oceanic basalts: implications for mantle composition and processes. In: Saunders, A. D. & Norry, M. J. (eds) *Magmatism in the Ocean Basins. Geological Society, London, Special Publications* **42**, 313–345.

Takahashi, E. & Kushiro, I. (1983). Melting of a dry peridotite at high pressures and basalt magma genesis. *American Mineralogist* **68**, 859–879.

Tatsumi, Y., Hamilton, D. J. & Nesbitt, R. W. (1986). Chemical characterization of fluid phase released from a subducted lithosphere and origin of arc magmas: Evidence from high-pressure experiments and natural rocks. *Journal of Volcanology and Geothermal Research* **29**, 293–309.

Thirlwall, M. F., Upton, B. G. J. & Jenkins, C. (1994). Interaction between continental lithosphere and the Iceland plume—Sr–Nd–Pb isotope geochemistry of Tertiary basalts, NE Greenland. *Journal of Petrology* **35**, 839–879.

Timm, C., Hoernle, K., van den Bogaard, P., Bindeman, I. & Weaver, S. (2009). Geochemical evolution of intraplate volcanism at Banks Peninsula, New Zealand: Interaction between asthenospheric and Lithospheric melts. *Journal of Petrology* **50**, 1–35.

Turner, S., Sandiford, M. & Foden, J. (1992). Some geodynamic and compositional constraints on 'postorogenic' magmatism. *Geology* **20**, 931–934.

Turner, S. & Hawkesworth, C. J. (1995). The nature of the sub-continental mantle: constraints from the major element composition of continental flood basalts. *Chemical Geology* **120**, 295–314.

Turner, S., Arnaud, N., Liu, J., Rogers, N., Hawkesworth, C., Harris, N., Kelley, S., van Calsteren, P. & Deng, W. (1996). Post-collisional, shoshonitic volcanism on the Tibetan Plateau: implications for convective thinning of the lithosphere and the source of ocean island basalts. *Journal of Petrology* **37**, 45–71.

Turner, S., Hawkesworth, C., van Calsteren, P., Heath, E., Macdonald, R. & Black, S. (1997). U-series isotopes and destructive plate margin magma genesis in the Lesser Antilles. *Earth and Planetary Science Letters* **142**, 191–207.

Turner, S., Platt, J. P., George, R. M. M., Kelley, S. P., Pearson, D. G. & Nowell, G. M. (1999). Magmatism associated with orogenic collapse of the Betic–Alboran Domain, SE Spain. *Journal of Petrology* **40**, 1011–1036.

Turner, S. P. (2002). On the time-scales of magmatism at island-arc volcanoes. *Philosophical Transactions of the Royal Society of London, Series A* **360**, 2853–2871.

Weaver, B. L. (1991). The origin of ocean island basalt end-member compositions: trace element and isotopic constraints. *Earth and Planetary Science Letters* **104**, 381–397.

Wang, K. L., Chung, S. L., O'Reilly, S. Y., Sun, S. S., Shinjo, R. & Chen, C. H. (2004). Geochemical constraints for the genesis of post-collisional magmatism and the geodynamic evolution of the northern Taiwan region. *Journal of Petrology* **45**, 975–1011.

Weis, D., Kieffe, B., Maersschalk, C., Pretorius, W. & Barling, J. (2005). High-precision Pb–Sr–Nd–Hf isotopic characterization of USGS BHVO-1 and BHVO-2 reference materials. *Geochemistry, Geophysics, Geosystems* **6**, Q02002, doi:10.1029/2004GC000852.

Weis, D., Kieffer, B., Maerschalk, C., Barling, J., de Jong, J., Williams, G. A., Hanano, D., Pretorius, W., Mattielli, N., Scoates, J. S., Goolaerts, A. & Friedman, R. M. (2006). High precision isotopic characterization of USGS reference materials by TIMS and MC–ICP-MS. *Geochemistry, Geophysics, Geosystems* **7**, doi:10.1029/2006GC001283.

Yılmaz, Y. (1993). New evidence and model on the evolution of the southeast Anatolian orogeny. *Geological Society of America Bulletin* **105**, 252–271.

Yılmaz, Y., Şaroğlu, F. & Güner, Y. (1987). Initation of the neomagmatism in East Anatolia. *Tectonophysics* **137**, 177–199.

Yılmaz, Y., Güner, Y. & Şaroğlu, F. (1998). Geology of the Quaternary volcanic centres of the East Anatolia. *Journal of Volcanology and Geothermal Research* **85**, 173–210.

Zindler, A. & Hart, S. R. (1986). Chemical geodynamics. *Annual Review of Earth and Planetary Sciences* **14**, 493–571.

Zor, E., Sandvol, E., Gurbuz, C., Turkelli, N., Seber, D. & Barazangi, M. (2003). The crustal structure of East Anatolian plateau from receiver functions. *Geophysical Research Letters* **30**, doi:10.1029/2003GL018192.

Downloaded from https://academic.oup.com/petrology/article-abstract/55/1/37/1524170 by Yuzuncu Yil University user on 23 April 2020